JRC Scientific and Technical Reports

Uranium Migration in Crystalline Rocks

.

W. E. Falck, D. Read, S. Black, D. Thornley, M. Siitari-Kauppi

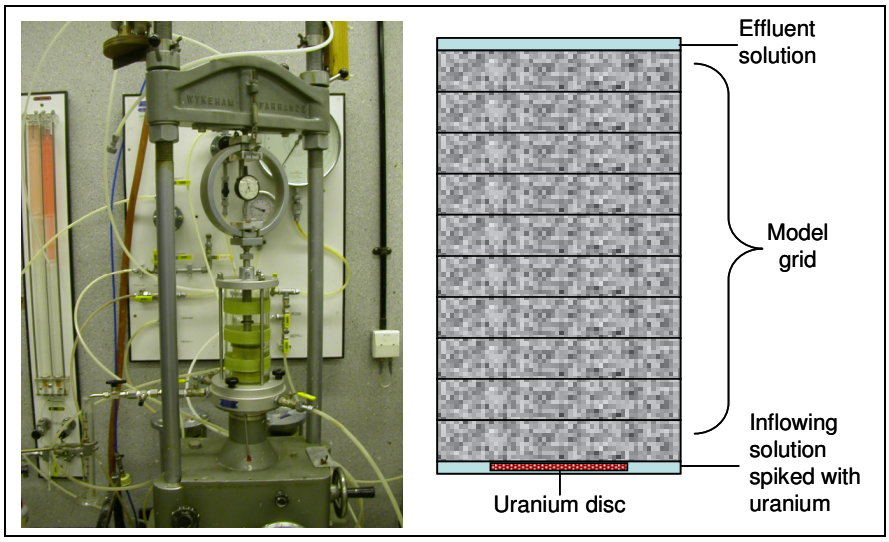

EUR 23816 EN - 2009

JRC EUROPEAN COMMISSION
Institute for Energy

The mission of the JRC-IE is to provide support to Community policies related to both nuclear and non-nuclear energy in order to ensure sustainable, secure and efficient energy production, distribution and use.

European Commission
Joint Research Centre
Institute for Energy

Contact information
Address: P.O. Box 2, NL-1755 ZG Petten, The Netherlands
E-mail: eberhard.falck@jrc.nl
Tel.: +31-224-56-5214
Fax: +31-224-56-5641

http://ie.jrc.ec.europa.eu/
http://www.jrc.ec.europa.eu/

JRC50583

EUR 23816 EN
ISBN 978-92-79-12346-7
ISSN 1018-5593
DOI 10.2790/11199

Luxembourg: Office for Official Publications of the European Communities

Printed in Luxembourg

Executive Summary

The mechanisms controlling the migration of uranium in crystalline rocks, such as granites or granodiorites, are still insufficiently well understood to arrive at a quantitatively defensible safety case for deep disposal of radioactive waste based on numerical modelling alone. To help further our knowledge of the relevant processes, a controlled column experiment was undertaken using a disc of metallic (depleted) uranium as a source and granodiorite samples from a former candidate disposal site for spent uranium fuel, Sievi in Finland, as the host medium. The experiment ran for approximately 500 days.

This report summarises efforts made to simulate the uranium migration observed during the experiment. Initial models were constructed with minimal information in order to replicate the situation faced by workers in the early stages of a deep disposal programme. First stage, 'blind' predictions typically utilise generic information for testing conceptual models of the system. Conceptual and numerical model are then refined using site-specific information as it becomes available. At the same time, the predictions are used to guide the experimental programme, identifying data needs and the key uncertainties.

Initial 'blind' modelling efforts using the PHREEQC geochemical code and literature data pointed to several solid phases that potentially control the solubility of uranium. As experimental data became available, the model could be refined, but the initial assumptions were corroborated in principle. The model points to hydrous uranium silicates as likely solubility controlling phases. A slight supersaturation with respect to iron-oxyhydroxides may give rise to the possibility that these may influence uranium concentrations by co-precipitation or sorption.

It proved difficult to constrain the model and to arrive at unique solutions even for this relatively simple, controlled experimental system. Several variables, for example the precipitation kinetics of individual solid phases and the dispersivity of the system, merit further investigation. Comparison of model results with the measured effluent concentrations clearly demonstrated the limitations of an equilibrium speciation code.

The experiment revealed a number of unexpected features that could not have been predicted in advance. Consequently, it is very difficult to state *a priori* whether a given simulation will yield conservative results.

Contents

Executive Summary 3
Contents 4
1. Introduction 5
2. Experimental work 5
  2.1 Rationale 5
  2.2 Column migration experiments 5
3. Conceptual model considerations 6
4. Blind predictions 7
  4.1 Initial water compositions 7
  4.2 Estimating the hydraulic properties of the experimental system 8
  4.3 Results of hydrodynamic calculations 10
  4.4 Dual porosity model 10
  4.5 Solubility controlling phases for uranium 16
  4.6 Modelling uranium dissolution 17
  4.7 Modelling uranium migration 18
  4.8 Precipitation kinetics 21
5. Re-running the model with experimental data 23
  5.1 Initial water composition 23
  5.2 Hydraulic model 24
  5.3 Uranium migration 25
  5.4 Major ion chemistry 29
6. Comparison with experimental data 30
  6.1 Flow data 30
  6.2 Effluent composition 32
  6.3 Static PHREEQC simulations using the experimental data 34
  6.4 Reactive transport simulations 35
7. Summary and Conclusions 40
9. References 41

1. Introduction

Geological disposal is the preferred management end-point for high-level waste and, in some countries, also for spent fuel. A safety assessment procedure has to demonstrate for a given case that any releases of radionuclides that will almost certainly occur at some time in the future have negligible impact; in the short term this equates to dose to critical groups remaining below acceptable levels.

The safety assessment procedure is made up of various components that are designed to represent the behaviour of the repository itself and the surrounding geological environment, and to predict its behaviour far into the future. Thus, both its mechanistic behaviour and the stochastic variability of properties and processes have to be described in a quantitative way.

Although a large body of quantitative information on possible rock matrices for disposal and on pertinent processes and events has been accumulated over the past 30 years, many processes have not yet been adequately characterised. In particular, the geochemical behaviour of transuranic elements in general and the micro-scale behaviour of elements such as uranium are insufficiently known. The complex redox chemistry of these elements makes them sensitive to changing geochemical conditions with respect to their migration or retention behaviour.

Detailed process knowledge is required as a basis for informed simplification as required by performance assessment codes. This process knowledge can be developed inter alia through well-defined experimental programmes.

2. Experimental work

2.1 Rationale

Experimental programme to understand uranium and transuranium element migration in crystalline host rock usually have to be carried out at different scales in order to allow verification of the simplifying assumptions made during the upscaling process. This upscaling is necessary when moving from mechanistic, process-oriented models to larger-scale performance assessment models.

This report discusses the efforts made to model a migration experiment that was undertaken at the mm-scale on a granodiorite sample from Sievi in Finland. Parallel field studies in southern Finland provide essential calibration to the physical and temporal scales relevant for geological disposal (READ *et al.*, 2007).

The migration experiment was undertaken at the University of Reading (Prof. David Read, D. Thornley, S. Black), UK, on a Sievi-Granodiorite sample provided by the Helsinki Technical University (Dr. Marja Siitari-Kauppi) and prepared by Antero Lindberg (GTK).

2.2 Column migration experiments

In the laboratory experiment, a disc cut from a depleted uranium (DU) penetrator (armour piercing ammunition) is placed between two slices of granodiorite in a triaxial cell (Figure 1a). In addition to a confining pressure, a slight upward directed flow is imposed. Owing to the fact that the DU used contains some uranium derived from reprocessing, trace quantities of plutonium and other transuranic elements are present (TRUEMAN *et al*., 2004).

The basic aqueous chemistry of uranium and the transuranics is reasonably well known, but their geochemical behaviour still poses many questions. Previous studies (TRUEMAN *et al*., 2005*;* BAUMANN *et al*., 2006) demonstrate the rapid degradation of the DU discs under a range of experimental

conditions when exposed to excess solution. In the experiment carried out at the University of Reading, rock-solution ratios are more representative of those in the field and, in addition, the fate of the radionuclides released was assessed. While the experiment generated two basic sets of data, namely the chemical composition of the effluent as a function of time and data from destructive analyses of the rock samples upon termination of the experiment, this report discusses the efforts to model the measured effluent data.

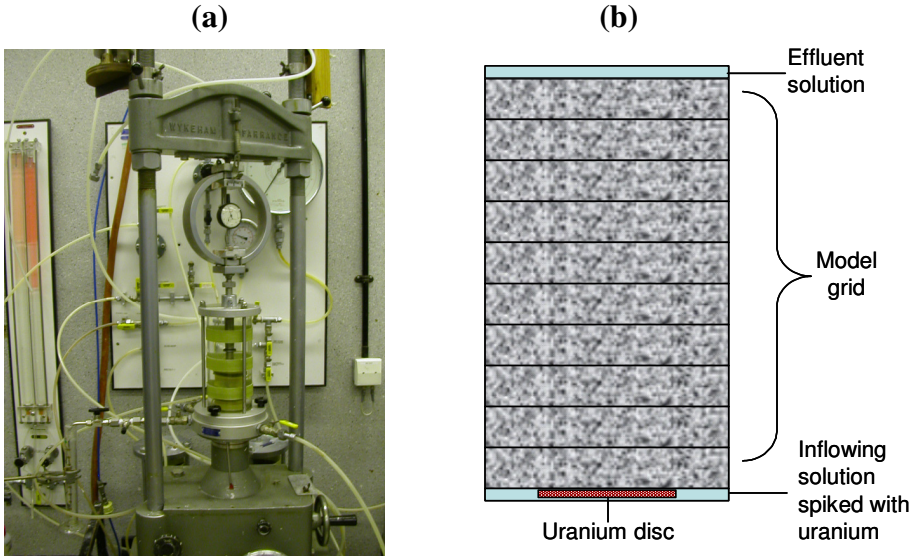

Figure 1: (a) Experimental set-up at Reading university and (b) conceptual layout of model.

3. Conceptual model considerations

Given the complexity of coupled geochemical transport processes, quantitative evaluation of the experiments can only be achieved by numerical computer modelling. Different modelling strategies can be followed. These include two-step, reactive geochemical modelling for particular domains in time and space, as well as coupled reactive-transport modelling in order to mimic the actual processes taking place.

The most useful method of evaluating such experiments is to begin with blind predictions first, since this approach challenges the modeller to document the assumptions employed in scenario construction (READ, 1991; BRUNO *et al.*, 1999). The modeller starts with the absolute minimum of information and very simple conceptual and numeric models. The models are gradually refined and parameter values constrained as information becomes available, the aim being to progressively reduce model uncertainties. As the modelling process inherently involves sensitivity analyses, it also helps to identify those mechanisms and processes that are crucial and that need to be parameterised with a greater level of confidence.

The simplest model for a column is a 'black-box' model, *i.e.* a zero-dimensional, one-cell model with defined upper and lower boundary conditions; this is essentially an input-output function model. Owing to the lack of any spatial resolution, it is not possible to distinguish between different mechanisms that may determine an output function. Thus, for instance, it is not possible to distinguish between the effects of hydrodynamic dispersion and reaction kinetics; both will lead to a 'smearing out' of output concentrations when compared to the input concentration profile.

For the above reasons, it was considered more informative to use a one-dimensional model with several cells. In such a model (effective) porosities and dispersion lengths can be varied and their effect compared to the effects of different chemical processes. Figure 1 illustrates the conceptual model that was used for the experimental set-up described above. For calculational purposes the cores

were subdivided into 10 cells. This allows depth profiles to be analysed and likely retention mechanisms to be assessed in some spatial detail.

In blind predictions and depending on the starting point chosen, nothing may be known even about the initial water composition and any reactions that may take place within the column. Assumptions regarding newly formed secondary phases incorporating the radionuclide of interest may have to be derived from earlier experimental evidence, 'analogues' or literature data. The major adjustable variables, in addition to those governing the hydraulic properties, will be the nature and properties of solubility controlling solid phases. The model will be refined with experimental data, thus arriving at a more realistic input-output estimate. The latter may include estimates of kinetics. After termination of the actual experiments and analysis of the solids, these results can be compared with the predictions from the model.

The code PHREEQC (PARKHURST & APPELO, 1999; version 2.12.5) was chosen as the numerical tool. The code offers in addition to the well-established chemical models a one-dimensional mixing cell model. The mixing cell model has some disadvantages when modelling hydrodynamic processes (see discussion below), but these are outweighed by the rather sophisticated options for the chemical processes. The chemical calculations were performed using the Lawrence Livermore Laboratory thermodynamic database (of 02.02.2002) that is delivered together with the code.

4. Blind predictions

4.1 Initial water compositions

As indicated above, before assimilating the actual experimental data (inverse model), an attempt at blind prediction was made. Consequently literature data for a granitic groundwater from Äspö (LAAKSOHARJU, 1997, as quoted in BRUNO *et al.*, 1999) were used for the initial water composition (Table 1).

The actual experiment is being run using water pre-equilibrated with crushed Sievi granodiorite, from the same location as that in the triaxial cell. Equilibrium with atmospheric CO_2 must be assumed for the laboratory experiments and is used to determine the alkalinity, which then also determines the system redox potential.

Table 1: Äspö groundwater compositions (LAAKSOHARJU, 1997).

Component	Concentration [mol/dm³]
Na^+	$9.13 \cdot 10^{-2}$
K^+	$2.05 \cdot 10^{-4}$
Ca^{2+}	$4.73 \cdot 10^{-2}$
Mg^{2+}	$1.73 \cdot 10^{-3}$
Fe^{2+}	$4.30 \cdot 10^{-6}$
Mn^{2+}	$5.28 \cdot 10^{-6}$
H_4SiO_4	$1.46 \cdot 10^{-4}$
HCO_3^-	$1.64 \cdot 10^{-4}$
F^-	$7.89 \cdot 10^{-5}$
Cl^-	$1.81 \cdot 10^{-4}$
SO_4^{2-}	$5.83 \cdot 10^{-3}$
pH	7.7
Eh [mV]	-300

Initial calculation with PHREEQC and the Lawrence Livermore National Laboratory thermodynamic database (tdb) show that the water is close to equilibrium with respect to albite, quartz and several clay minerals, reflecting the main constituents of granite. The following runs were set up so that equilibrium with H-saponite was maintained, which provides for some silicate and pH-buffering in the system.

Further, according to the data in Table 1, the infiltrating solution was brought into equilibrium with O_2 and CO_2 at their respective atmospheric partial pressures. It was found that the resulting water composition would be slightly supersaturated with respect to ferric hydroxide and, hence, precipitation of it was allowed. This provides for additional pH-buffering. The ferric hydroxide might also provide a substrate for adsorption of uranium species. However, this process was not yet modelled, since the possibility of forming of such precipitates needs to be confirmed using the experimental data first.

4.2 Estimating the hydraulic properties of the experimental system

The experimental set-up consists of a triaxial cell into which two core sections of Sievi granodiorite from Finland of 49.5 mm diameter and 47.34 mm length were placed. The flow rate for the given set-up was determined to be 0.017 cm^3/min in a blank test.

The porosity of the two samples used was 9.1% and 13.6% respectively by the helium method. An average value of 10% for the total porosity (n_{tot}) was assumed in the following calculations. In absence of a tracer test, the effect of different effective porosities (n_e) was explored by assuming that the effective porosity equals the total porosity (i.e. $n_e = n_{tot} = 10\%$) and is 10% of the total porosity (i.e. $n_e = 0.1 \times n_{tot} = 1\%$), as upper and lower bounds respectively.

Advective-dispersive-diffusive transport is calculated in PHREEQC using a mixing cell model. The resulting transport equations are solved with an explicit finite difference scheme that is forward in time, central in space, and upwind in advective transport (PARKHURST & APPELO, 1999). This has to be kept in mind, when setting up the model system. The governing equation is the classical partial differential equation for advective, dispersive and diffusive transport:

$$\frac{\partial C}{\partial t} = -\nu \frac{\partial C}{\partial x} + D_L \frac{\partial^2 C}{\partial x^2} - \frac{\partial q}{\partial t}, \qquad [1]$$

where t is the time, ν is the average porewater flow velocity, x, the distance, D_L the hydrodynamic dispersion coefficient and q a source term and where

$$D_L = D_m + \alpha_L \nu \qquad [2]$$

with D_m the molecular diffusion coefficient and α_L the dispersion length. Equation 2 permits a sensitivity analysis to check whether transport would be diffusion or dispersion controlled for a given porewater velocity.

The mixing cell model in PHREEQC does not allow the effective porosity to be entered explicitly, rather it has to be entered implicitly via the average porewater flow velocity. Thus, the cells are modelled as a continuum and as stream tubes. Using the physical data given above, average porewater flow velocities can be calculated (Table 2), which in turn are used to determine the length of the time steps in the model. The time steps were rounded to give convenient numbers for scaling on an hourly basis.

Table 2: Selection of parameter values for transport simulation in PHREEQC for a cell length of 4.734 mm.

Run	Total porosity n_{tot}	Effective porosity n_e	Dead-end porosity	Dispersion length α_L [mm]	Flow-rate [m^3/s]	Cross-section [m^2]	Effective cross-section [m^2]	Average water velocity [m/s]	Calculated time step [s]	Selected time step [s]	Shape factor	Pore Radius [m]
SP1	0.1	0.1	0	0.5	$2.833 \cdot 10^{-10}$	$1.924 \cdot 10^{-3}$	$1.924 \cdot 10^{-4}$	$1.472 \cdot 10^{-6}$	32154	36000	n/a	$2.475 \cdot 10^{-3}$
SP2	0.05	0.05	0	0.5	$2.833 \cdot 10^{-10}$	$1.924 \cdot 10^{-3}$	$9.620 \cdot 10^{-5}$	$2.945 \cdot 10^{-6}$	16073	18000	n/a	$1.237 \cdot 10^{-3}$
SP2a	0.05	0.05	0	5.0	$2.833 \cdot 10^{-10}$	$1.924 \cdot 10^{-3}$	$9.620 \cdot 10^{-5}$	$2.945 \cdot 10^{-6}$	16073	18000	n/a	$1.237 \cdot 10^{-3}$
SP2b	0.05	0.05	0	0.05	$2.833 \cdot 10^{-10}$	$1.924 \cdot 10^{-3}$	$9.620 \cdot 10^{-5}$	$2.945 \cdot 10^{-6}$	16073	18000	n/a	$1.237 \cdot 10^{-3}$
SP2c	0.05	0.05	0	0	$2.833 \cdot 10^{-10}$	$1.924 \cdot 10^{-3}$	$9.620 \cdot 10^{-5}$	$2.945 \cdot 10^{-6}$	16073	18000	n/a	$1.237 \cdot 10^{-3}$
SP2d	0.05	0.05	0	0	$2.833 \cdot 10^{-10}$	$1.924 \cdot 10^{-3}$	$9.620 \cdot 10^{-5}$	$2.945 \cdot 10^{-6}$	16073	18000	n/a	$1.237 \cdot 10^{-3}$
SP3	0.01	0.01	0	0.5	$2.833 \cdot 10^{-10}$	$1.924 \cdot 10^{-3}$	$1.924 \cdot 10^{-5}$	$1.473 \cdot 10^{-5}$	3215	3600	1.500	$2.475 \cdot 10^{-4}$
SP4	0.09	0.09	0	0.5	$2.833 \cdot 10^{-10}$	$1.924 \cdot 10^{-3}$	$1.732 \cdot 10^{-4}$	$1.636 \cdot 10^{-6}$	28932	28800	1.500	$2.227 \cdot 10^{-3}$
DP 1	0.1	0.05	0.05	0.5	$2.833 \cdot 10^{-10}$	$1.924 \cdot 10^{-3}$	$9.620 \cdot 10^{-5}$	$2.945 \cdot 10^{-6}$	16073	18000	1.500	$6.981 \cdot 10^{-4}$
DP 2	0.1	0.05	0.05	0.5	$2.833 \cdot 10^{-10}$	$1.924 \cdot 10^{-3}$	$9.620 \cdot 10^{-5}$	$2.945 \cdot 10^{-6}$	16073	18000	0.657	$6.981 \cdot 10^{-4}$
DP 3	0.1	0.01	0.09	0.5	$2.833 \cdot 10^{-10}$	$1.924 \cdot 10^{-3}$	$1.924 \cdot 10^{-5}$	$1.473 \cdot 10^{-5}$	3215	3600	1.500	$1.396 \cdot 10^{-4}$
DP 4	0.1	0.01	0.09	0.5	$2.833 \cdot 10^{-10}$	$1.924 \cdot 10^{-3}$	$1.924 \cdot 10^{-5}$	$1.473 \cdot 10^{-5}$	3215	3600	0.657	$1.396 \cdot 10^{-4}$
DP 5	0.1	0.09	0.01	0.5	$2.833 \cdot 10^{-10}$	$1.924 \cdot 10^{-3}$	$1.732 \cdot 10^{-4}$	$1.636 \cdot 10^{-6}$	28932	28800	0.657	$1.257 \cdot 10^{-3}$
DP 6	0.1	0.05	0.05	0.5	$2.833 \cdot 10^{-10}$	$1.924 \cdot 10^{-3}$	$1.924 \cdot 10^{-4}$	$1.473 \cdot 10^{-6}$	32147	36000	0.657	$6.981 \cdot 10^{-4}$

SP = runs with a single-porosity model; DP= runs with a dual porosity model.

Run SP 2d = plug flow, no molecular diffusion.

Similarly, the flow model as implemented in PHREEQC does not have any explicit knowledge of the lengths of flow paths or, in the present application, the length of any flow channels within the sample. The relative length of a straight tube reaching from one surface of the sample to the other, compared to the actual lengths of the flow paths is termed tortuosity. If there were a single tube, the tortuosity would be a single scaling factor. In practice, however, there will be a collection of flow paths of differing lengths so that the phenomenon of tortuosity is superimposed onto that of the hydrodynamic dispersion within the flow paths. The result is apparent retardation and a broadening of concentration peaks. In the absence of a tracer test, one can only perform a number of sensitivity analyses to scope this effect.

Inserting the basic data into Eq. 2 and comparing the magnitude of the two terms in it for $D_m = 0.3 \cdot 10^{-9}$ m^2/s and $v = 1.47 \cdot 10^{-6}$ m/s shows that for a (hydrodynamic) dispersion length of the order of 0.1 mm both terms would have equal weight in the transport equation.

A typical selection for a dispersion length in column experiments, if not determined experimentally through a tracer test, would be around 1/10 of the cell length for uniformly porous materials. In the present case this would amount to about 0.5 mm. In order to test the effect of dispersion length on the breakthrough of a tracer, calculations were performed by varying the dispersion length over several orders of magnitude.

Table 2 gives the set of parameter values selected for the simulations. The table in addition contains those variables that will be needed to model dual-porosity cases in PHREEQC as discussed below.

4.3 Results of hydrodynamic calculations

Scoping calculations have been performed for the various combinations of parameter values set out in Table 2. Figure 2 analyses the effect on tracer break-through of choosing various dispersion lengths. The time profiles for plug-flow (no longitudinal dispersion) with and without molecular diffusion are also shown. Figure 3 in turn shows the variation in break-through as a function of effective porosity for a dispersion length of 0.5 mm. Figure 4 briefly explores the effect of a tortuosity that leads to a doubling, on average, of the flow path lengths.

4.4 Dual porosity model

At present, the safety case for disposal of high level radioactive waste and spent nuclear fuel in fractured hard rocks relies heavily on the concept of dual porosity and the related concept of rock matrix diffusion (*e.g.* SKB, 2006). These assume that, although only a fraction of the total porosity, namely the effective porosity n_e, takes part in advective dispersive transport, there will be diffusive exchange between the fraction of porosity with mobile water and the fraction where water is immobile (n_i). This diffusive exchange will lower peak concentrations, but is also responsible for longer tails in concentration distributions.

The PHREEQC code allows dual-porosity cases to be calculated for various geometries. These geometries are introduced into the model via a 'shape factor'. For the case discussed here, a geometry was chosen whereby a stream-tube is embedded in a 1-layer deep tube of stagnant cells. Different thicknesses of the surrounding cells can be chosen. PARKHURST and APPELO, (1999) tabulate shape factors determined for this geometry and different depths. The factors range from 0.657 for a thickness that is equal to the pore radius to a factor of 1.5 for a thickness of 400 times the pore radius. Figure 5 illustrates the effect of different shape factors.

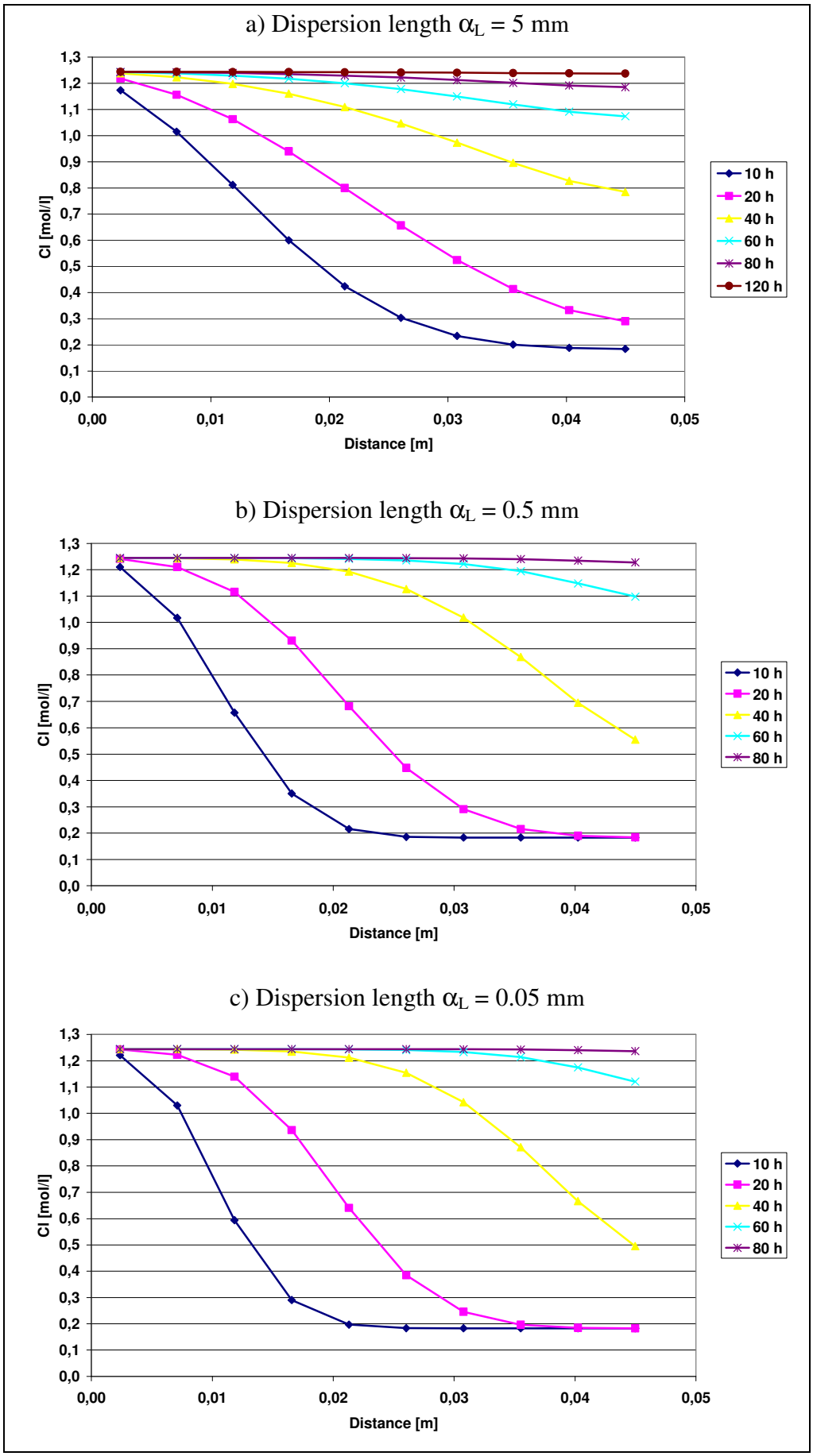

Figure 2: Tracer profiles for n_e=0.05 as a function of dispersion length α_l.

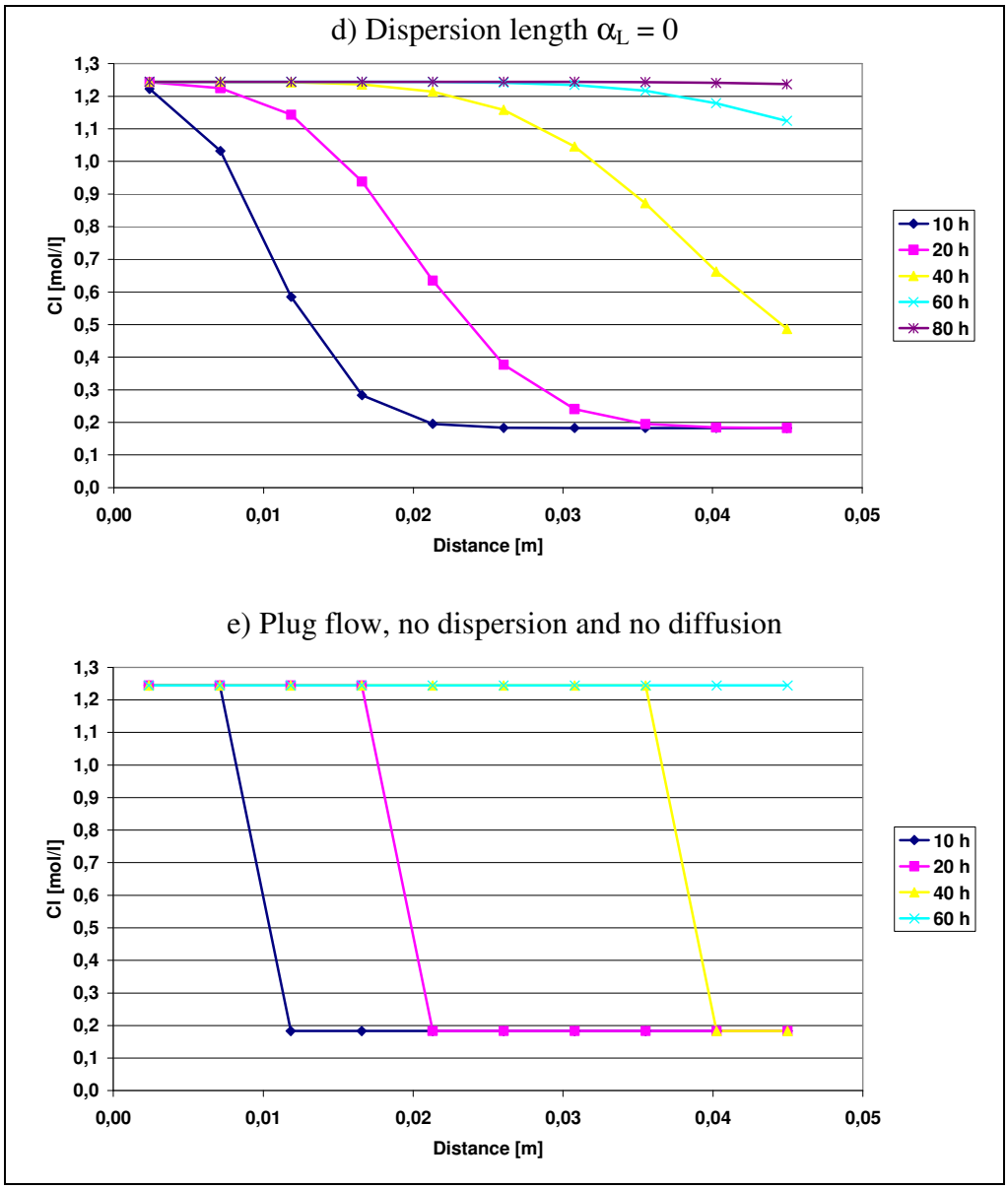

Figure 2, **continued**: Tracer profiles as a function of dispersion length α_l.

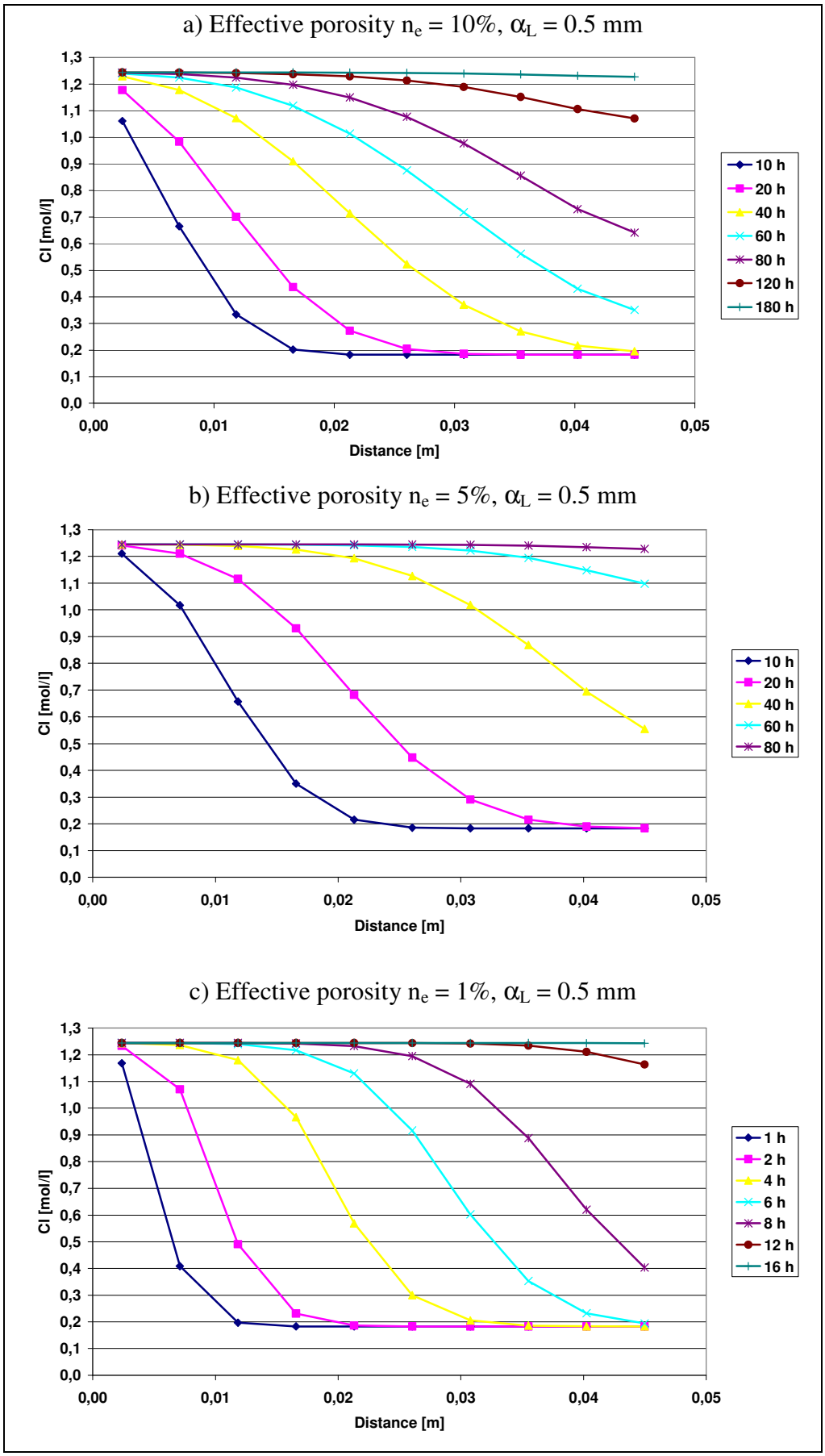

Figure 3: Tracer profiles as a function of effective porosity n_e.

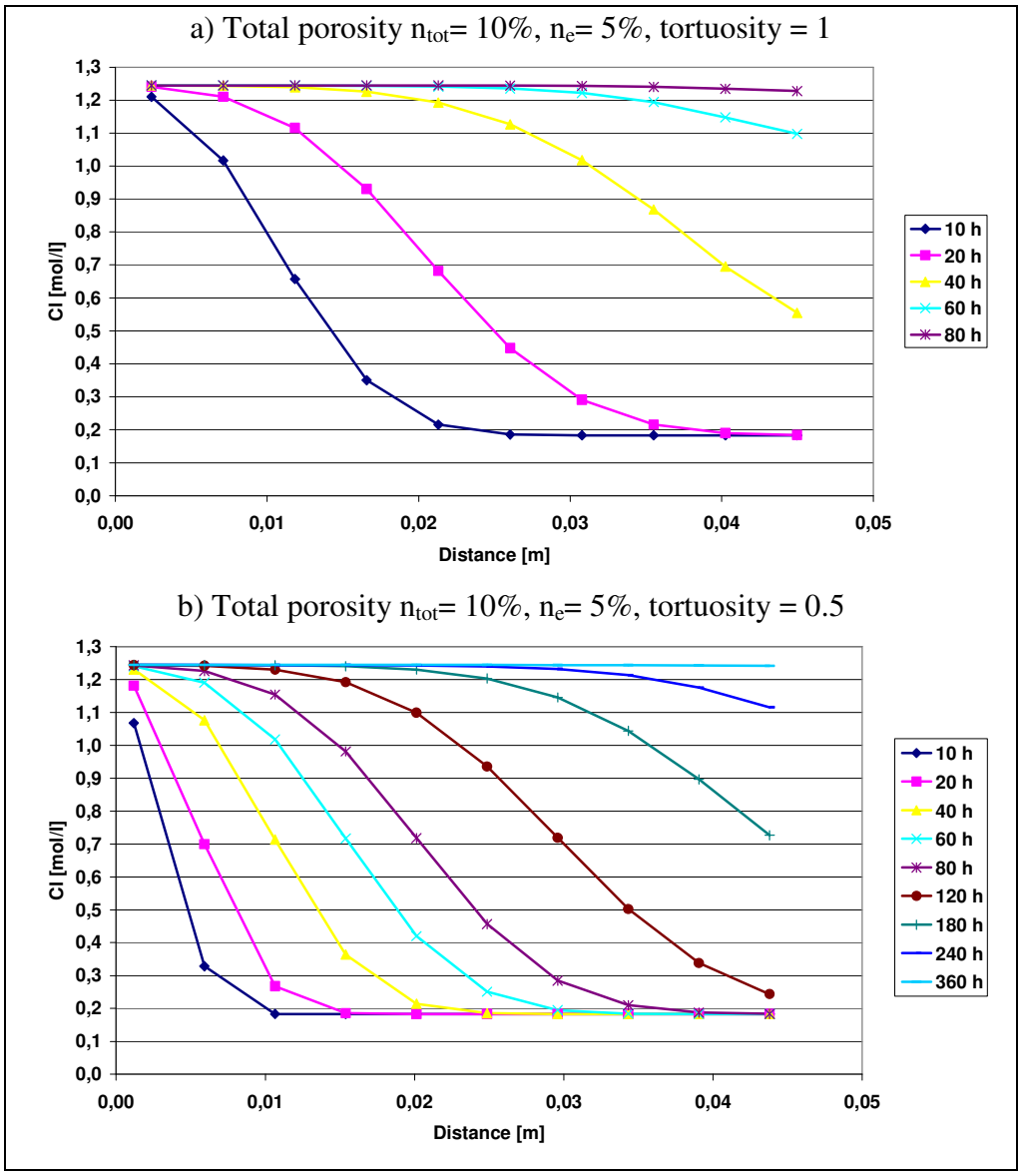

Figure 4: Tracer profiles for two different tortuosities.

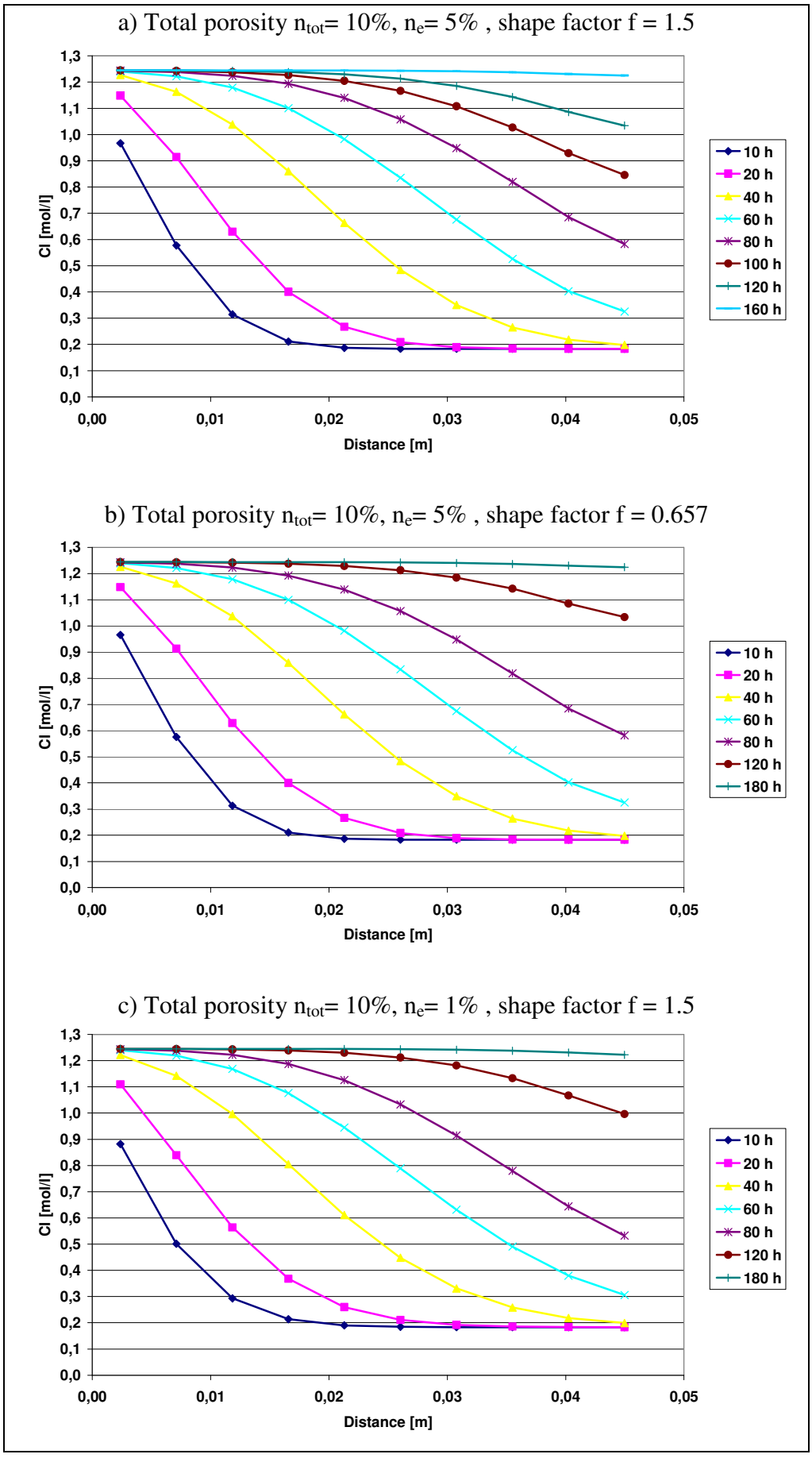

Figure 5: Tracer profiles for different combinations of effective porosity and shape factors in the dual porosity case.

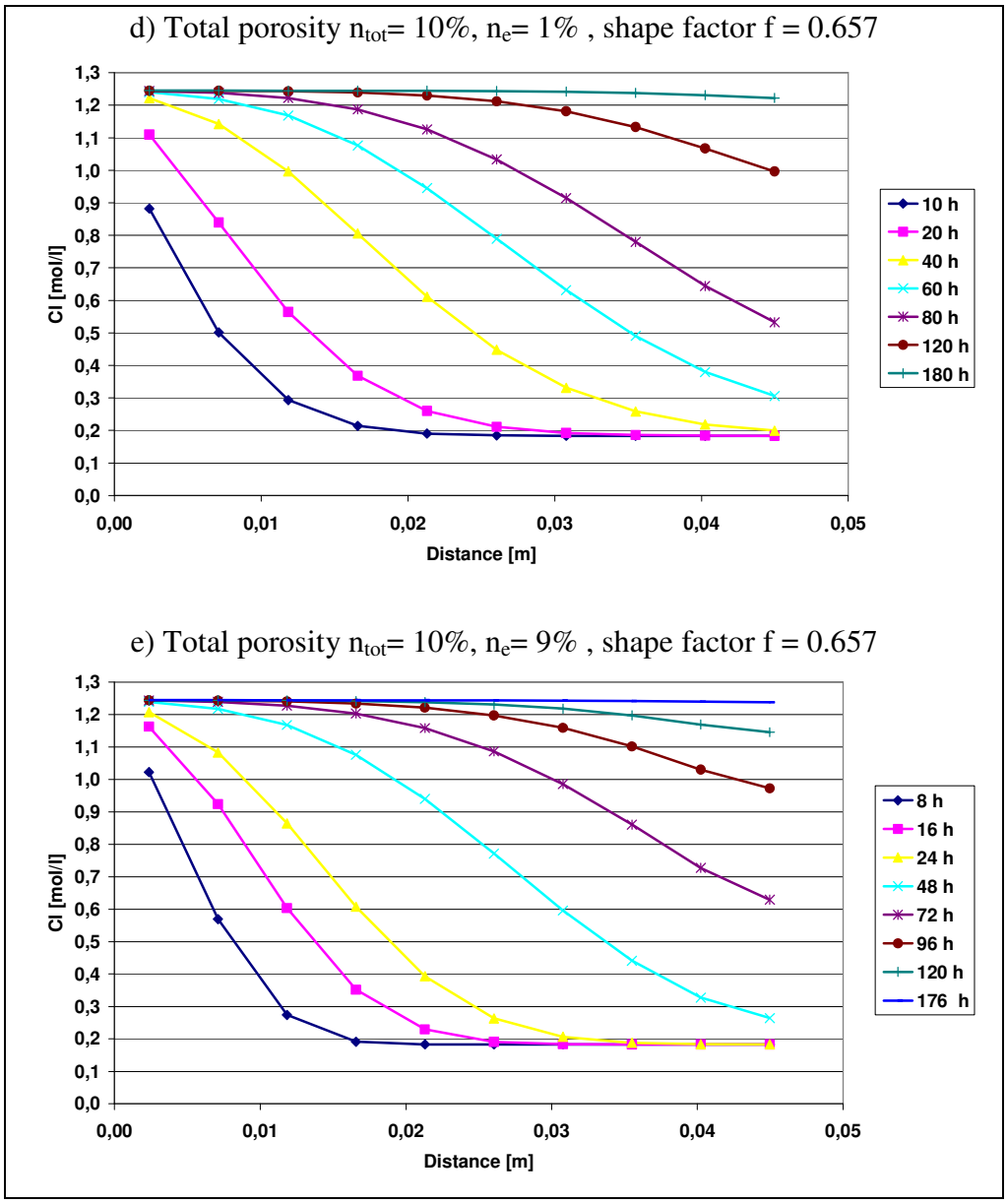

Figure 5, cont'd: Tracer profiles for different combinations of effective porosity and shape factors in the dual porosity case.

4.5 Solubility controlling phases for uranium

In order to scope potential secondary uranium phases that could control solubility in the column, batch experiments were simulated by adding incremental amounts of uranium to the solution from Table 1. Accordingly, the thermodynamically most stable phases are predicted to be $UO_2(OH)_2$ and $UO_3 \cdot nH_2O$ (schoepite) using the LLNL database. The latter may be polymorphous and have the formula $[(UO_2)_8O_2(OH)_{12}](H_2O)_{12}]$ (FINCH *et al.*, 1996). OSTANIN & ZELLER (2007) discuss in depth the crystal structure and various stages of hydration of schoepite (n= 2.25), meta-schoepite (n= 2) and dehydrated meta-schoepite (n=1.75). The LLNL database contains solubility products for $UO_3 \cdot nH_2O$ with n= 2, 1, 0.9, 0.85, 0.648 and 0.393.

$UO_3 \cdot nH_2O$ has, indeed, been identified as the dominant corrosion product from the dissolution of DU penetrators in soils (TRUEMAN *et al.* 2003; SHAW *et a*l., 2007). Considering the persisting uncertainty regarding relevant thermodynamic constants (see e.g. JANG *et al.*, 2006, for a recent review), it may suffice to conclude that for the given groundwater composition it will be a uranyl hydrous oxide (Figure 6). In the following calculation, schoepite is being used as a representative proxy.

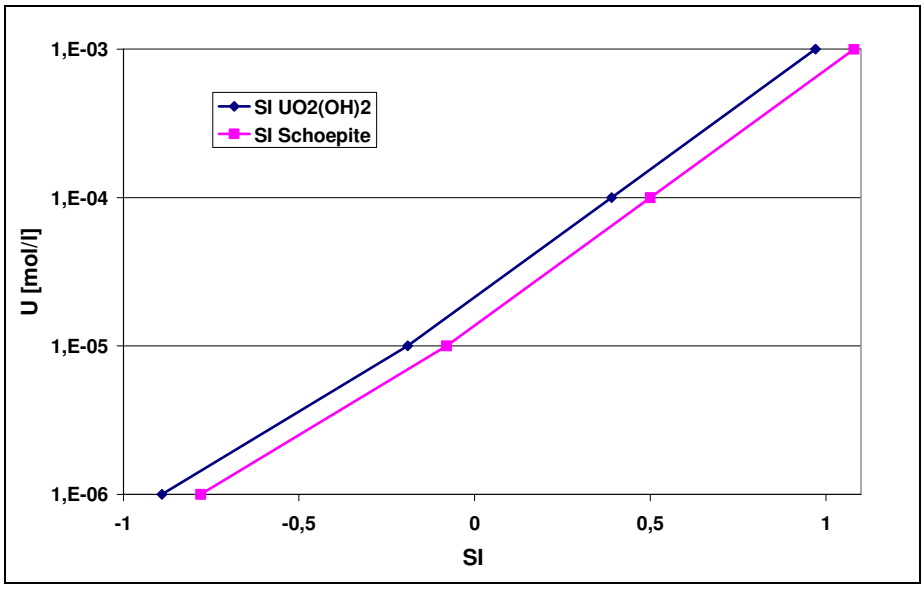

Figure 6: Saturation indices of $UO_2(OH)_2$ and schoepite as a function of total uranium added.

4.6 Modelling uranium dissolution

The uranium source was a disc cut from a depleted uranium (DU) penetrator (heavy tank projectile). The material was supplied by BAe Systems (Royal Ordnance Speciality Metals) in the form of 25 mm diameter discs, 0.5 mm in thickness. Hence, the total surface area of the source is 1021 mm^2 and the uranium mass is 4.688 g or 0.1674 moles.

It should be noted that spent nuclear fuel (with the exception of TRIGA fuel) does not contain uranium in its metallic form, but rather as an oxide. Therefore, the following considerations apply to understanding the source term in the experiment only and do not apply to repository conditions.

The summary equation for the dissolution of DU metal is for the aerobic case:

$$U_c + 3H_2O + 1.5O_2 \rightarrow UO_2^{2+} + 6OH^- \quad [3]$$

and under anaerobic conditions:

$$U_c + 2H_2O \rightarrow UO_2 + 2H_2^{\uparrow} \quad [4]$$

In the absence of carbonate ions and at sufficiently high concentrations to exceed the respective solubility product, the uranyl ions would precipitate as hydrous uranyl oxides.

In terms of the PHREEQC notation Equation 3 needs to be written as:

$$U_c + 2\ H_2O \rightarrow UO_2^{2+} + 6\ H^+ + 6\ e^- \quad [5]$$

The LLNL-database does not contain data for reaction 5. Attempts were therefore undertaken to obtain suitable literature data. OSTANIN & ZELLER (2007), for instance, provide calculated enthalpy data for the formation of schoepite and meta-schoepite from the elements (at T= 0 K only):

$$U_c + 2.25\ H_2 + 2.625\ O_2 \rightarrow [UO_3 \cdot 2.25\ H_2O]_{schoepite} \qquad \Delta H = -1769\ kJ/mol \quad [6]$$

$$U_c + 2.00\ H_2 + 2.500\ O_2 \rightarrow [UO_3 \cdot 2.00\ H_2O]_{meta\text{-}schoepite} \qquad \Delta H = -1690\ kJ/mol \quad [7]$$

According to the LLNL-database, the enthalpy of formation of schoepite from the respective 'master' species is (at T= 298 K)

$UO_3 \cdot 2.00\ H_2O + 2\ H^+ \leftrightarrow UO_2^{2+} + 3\ H_2O$ ΔH= -1826.1 kJ/mol [8]

Reaction 7 can be rewritten using the appropriate equations for the formation of H_2 and O_2 from the master species as used in PHREEQC:

$O_2 \leftrightarrow 2\ H_2O - 4\ H^+ - 4\ e^-$ ΔH= 2.9 kJ/mol [9]

$2\ H_{2(g)} \leftrightarrow 2\ H_2O - O_2$ ΔH= -8.368 kJ/mol [10]

to give

$U_c + 5\ H_2O - 6\ H^+ - 6\ e^- \rightarrow [UO_3 \cdot 2.00\ H_2O]_{meta\text{-}schoepite}$ ΔH= -1688.9 kJ/mol [11]

Combining Reactions 11 and 8 leads to Reaction 5, which is – in terms of PHREEQC master species - the oxidation of metallic uranium to the uranyl iron. One can estimate the associated enthalpy of reaction to be approximately ΔH= -3515 kJ/mol.

However, calculations had to stop here, as no appropriate ΔS values could be obtained from the literature that would have allowed to calculate the free energy of formation (ΔG) for reaction 11.

There are various ways of defining a dissolution reaction within PHREEQC, provided the necessary thermodynamic data are available. In present case a reaction rate constant can be defined. In the absence of these data, the reaction constituents can be added in fixed amounts or increments, which is akin to defining arbitrary dissolution kinetics with each calculation being performed for an arbitrary point in time. In this case, no feedback between solution composition and reaction rate can be simulated. However, a bulk average dissolution rate can be estimated, based on the total mass loss over the total experimental time.

For the purpose of the scoping calculations the following estimate has been made: given the total mass of 0.1674 moles of U in the disc, and assuming an experimental time of 180 days and a mass loss of 50% over that period, an approximate linear mass loss of $5.4 \cdot 10^{-9}$ mol/s can be calculated. This value has been used as a linear reaction rate for the blind predictions discussed below.

4.7 Modelling uranium migration

Based on the preliminary hydraulic assessment the further model runs were performed with values of 5% for the effective porosity and 0.5 mm for the dispersion length (see Figure 2b) respectively. In the tracer case these values indicate that the first detectable concentrations should be expected after a day in the experiment and steady state concentrations in the effluent by day 4. The time step in the model was 18000 s = 5 h. Calculations in PHREEQC are based on the mass of 1 kg of water, which for practical purposes here is equivalent to 1 dm^3. At an effective porosity of 5% the sample contains $4.55 \cdot 10^{-3}$ dm^3 mobile solution. Hence, to scale-up from the sample size to 1 dm^3 equivalent the arbitrary release rate of $5.4 \cdot 10^{-9}$ mol/s = $9{,}72 \cdot 10^{-5}$ mol/time step the amount of $2.134 \cdot 10^{-2}$ mol/time step must be used.

Since the initial volumetric flow rate was 0.017 cm^3/s, the arbitrary release rate of $5.4 \cdot 10^{-9}$ mol/s translates into a concentration of $3.176 \cdot 10^{-4}$ mol/dm^3 in the PHREEQC calculations for the solution moving into the column.

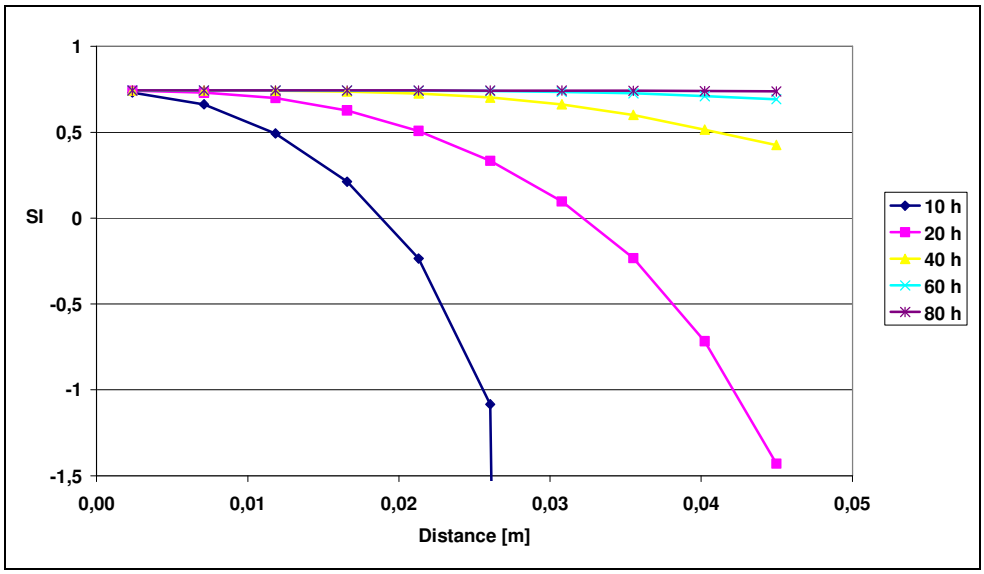

Figure 7: Saturation indices of schoepite as a function of distance into the core. The upper boundary conditions was a constant uranium concentration of $3.176 \cdot 10^{-4}$ mol/dm^3. No precipitation was allowed.

The calculations presented in Figure 7 show that at the assumed dissolution rate for DU and for the given water composition, saturation with respect to schoepite or $UO_2(OH)_2$ would be quickly reached. The model was set up in a way that precipitation would only occur within the granite core.

However, previous experiments have shown that alteration products accumulate on the surface of the DU discs (TRUEMAN *et al.*, 2003; BAUMANN *et al.*, 2006). The instantaneous (equilibrium) precipitation of schoepite as modelled in PHREEQC would result in no uranium above the equilibrium concentration, which is on the order of $3 \cdot 10^{-5}$ mol/dm^3, reaching the granite.

In order to observe uranium precipitation within the core, one must assume either that the alteration products formed on the DU penetrator have a higher solubility than secondary phases formed within the core, or that the precipitation is slow compared to the transport processes, or, indeed, a combination of these factors.

The data used to draw Figure 8 together with the molar volume of (meta-)schoepite allow the volume decrease in the open pore space due to the precipitation of this secondary mineral to be calculated. The density of schoepite is around 4.7 g/cm^3 (http://webmineral.com/data/Metaschoepite.shtml) and with a molecular weight of 313.05 g/mol this gives a molar volume of 66.61 cm^3/mol. This translates into a precipitated volume of 0.031 cm^3/day. In other words, the total pore volume of 9.6 cm^3 of the granite sample would be completely filled within just under 300 days. Of course, with increasing clogging of the pore volume the rate would fall. It needs to be verified on the sample where the formation of secondary minerals actually takes place. If the whole DU disc (=0,1674 mol U) were to be converted to schoepite, this would result in a volume increase from 2.5 cm^3 to 11 cm^3 that needs to be accommodated somewhere.

For the given water composition and assuming schoepite as the solubility controlling phase, the maximum uranium concentration in the column effluent would be around $3 \cdot 10^{-5}$ mol/l. For $UO_2(OH)_2$ this concentration would be slightly higher. Assuming instantaneous precipitation, i.e. as soon as SI= 0, results in the accumulation of uranium in the first cell of the model. With the given hydraulic conditions a steady state would be reached after about 60 h. In order to model the behaviour of uranium more realistically, some precipitation kinetics would need to be assumed.

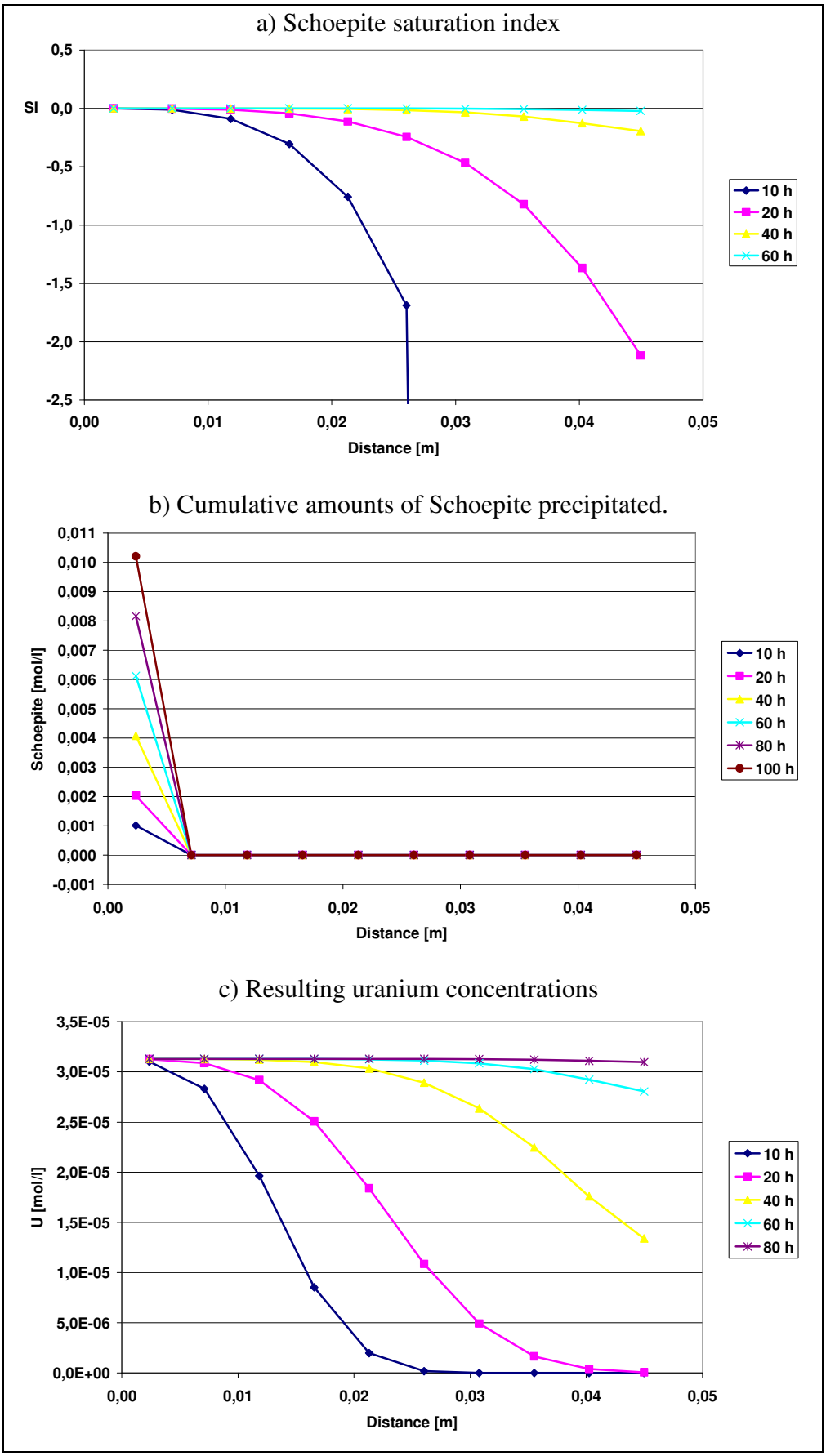

Figure 8: Flooding the core with a uranium solution of $3.176 \cdot 10^{-4}$ mol/dm^3 while allowing schoepite to precipitate.

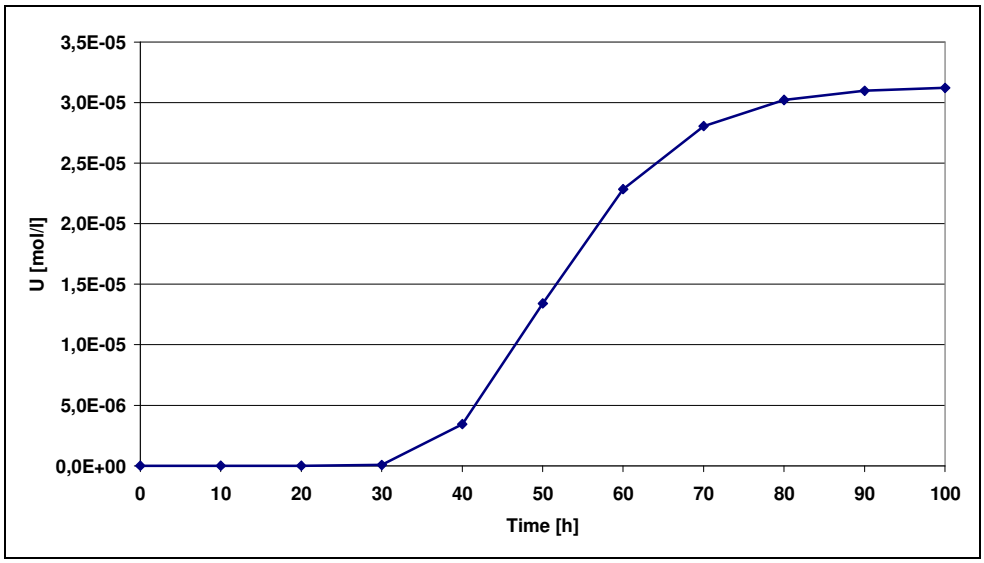

Figure 9: Effluent U concentrations at the end of the column as a function of time.

4.8 Precipitation kinetics

It is inherent in an equilibrium model that precipitation is instantaneous. Consequently, if no interaction with a pre-existing solid phase is modelled, complete precipitation in a column model will occur in the topmost cell. This kind of behaviour appears somewhat unrealistic and some precipitation deeper into the column should be expected due to slower precipitation kinetics.

PHREEQC allows different kinetic models and reaction rates for each cell in the model to be defined. The kinetic models can be written as subroutines in the BASIC programming language. These kinetic models and their parameterisation are usually derived from experimental data by curve-fitting exercises.

In a blind prediction case, however, no such data are available. Therefore, any modelling of precipitation kinetics is purely conjectural. In order to set up the model for later curve-fitting exercises and to demonstrate the effect of precipitation kinetics, a simple case with arbitrary kinetics was developed. It was assumed that the kinetics of precipitating schoepite would depend on the activity concentration of the uranyl ions in solution with different scaling factors (see Eq. 12).

$$R_{Schoepite} = r_f \cdot [UO_2^{2+}], \qquad [12]$$

where R is the reaction rate, r_f the scaling factor and square brackets denote activity; r_f was varied between 0.001 and 100. The results from these illustrative calculations are presented in Figure 10.

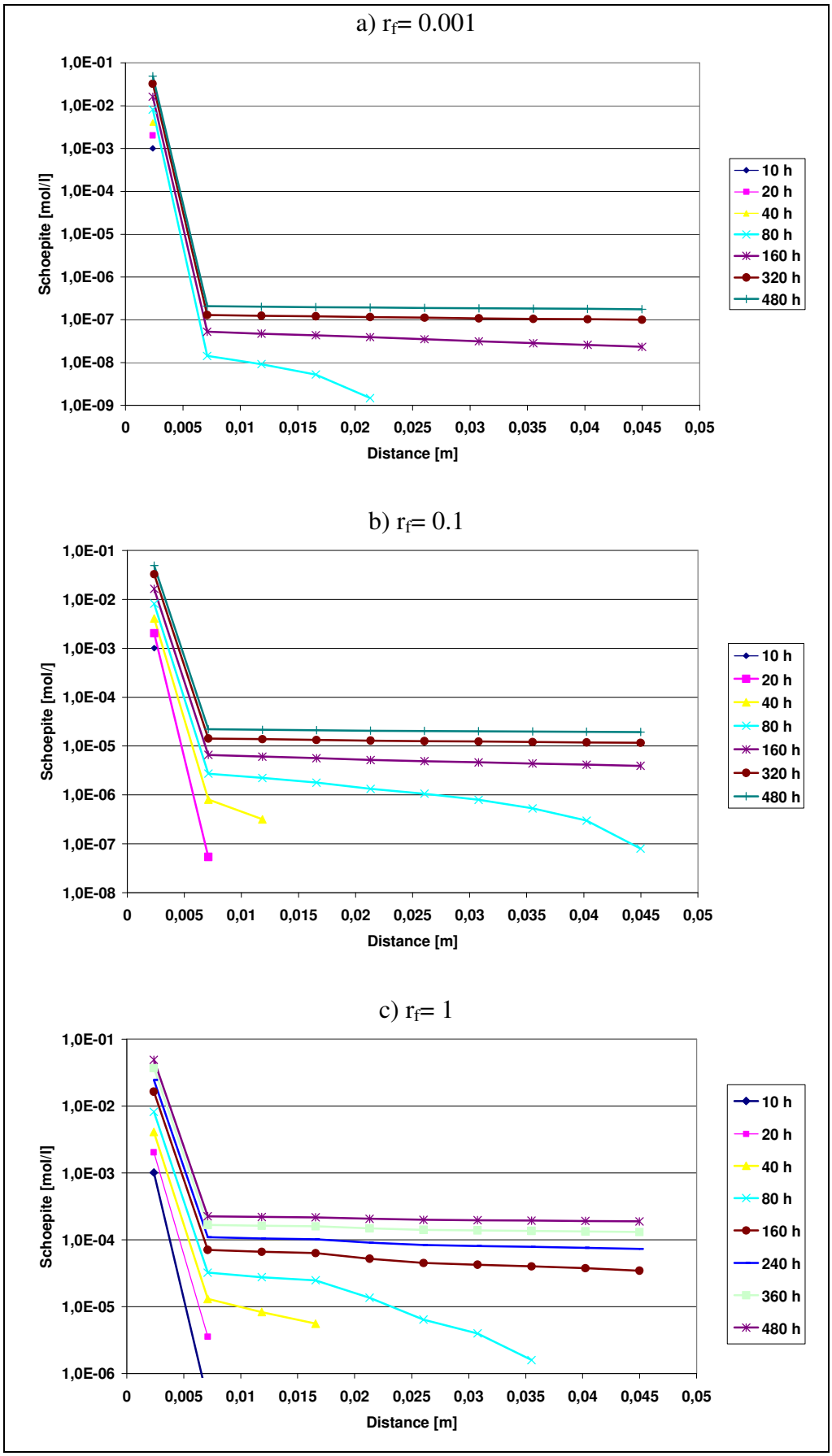

Figure 10: Schoepite precipitation along the column as a function of time and of the precipitation kinetics rate factors r_f .

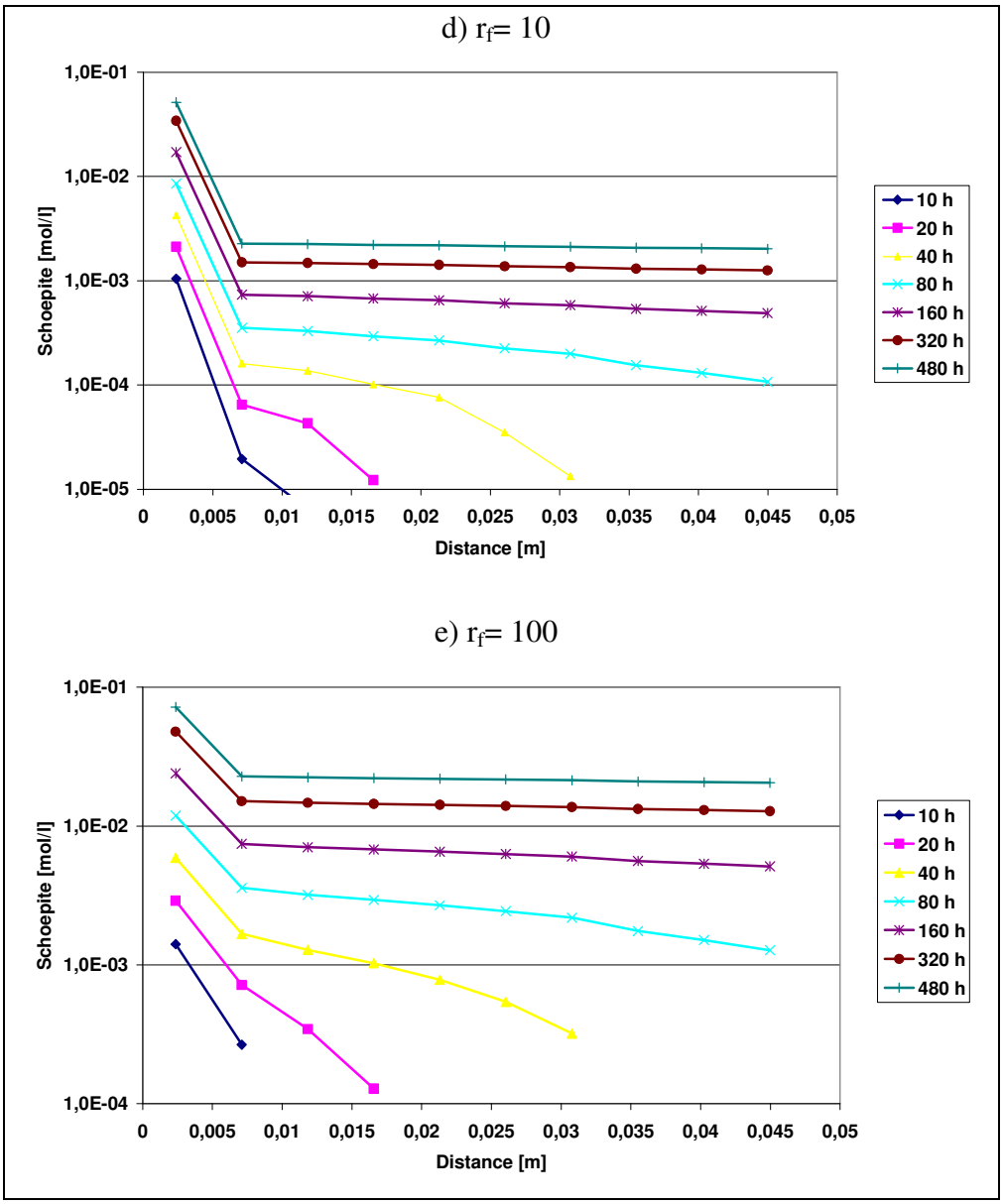

Figure 10, continued: Schoepite precipitation along the column as a function of time and of the precipitation kinetics rate factors r_f.

5. Re-running the model with experimental data

5.1 Initial water composition

In order to test the blind-predictions, the models were now re-run successively with experimental data. The measured inflow concentrations are given in Table 3.

These data differ from those for Äspö groundwater given in Table 1. The Äspö data show a greater influence of seawater due to proximity of the site to the Baltic coast. Chloride has not been determined in the above sample, but was used to balance the charge for the PHREEQC calculations. The high iron concentration appears to be some artefact, whether analytical or due to some contamination remains to be shown. It leads to a significant supersaturation with respect to ferric hydroxide that cannot simply be removed by letting it precipitate, as this would bring down the pH to a value of 3.4 in the absence of pH buffers.

Table 3: Experimental inflow concentrations of water pre-equilibrated with Sievi-Granodiorite [mol/l].

Component	measured	Component	measured
Na^+	$9.27 \cdot 10^{-4}$	HCO_3^-	not determined
K^+	$5.81 \cdot 10^{-5}$	PO_4^{3-}	$3.13 \cdot 10^{-6}$
Ca^{2+}	$8.85 \cdot 10^{-4}$	Cl^-	not determined
Mg^{2+}	$1.67 \cdot 10^{-3}$	SO_4^{2-}	$9.12 \cdot 10^{-5}$
Fe^{2+}	$1.33 \cdot 10^{-3}$	pH	6.64
Mn^{2+}	$8.45 \cdot 10^{-5}$	Eh [mV]	not determined
H_4SiO_4	$2.75 \cdot 10^{-5}$		

The lack of an effective buffering system in the aqueous phase becomes very obvious, when the solution is equilibrated with CO_2 at the atmospheric partial pressure. This leads to a drop of the pH to a value of 4.13, as initial calculations showed. The subsequent calculations focused on the identification of possible and likely buffer systems (Table 4). Calcite, as in the previous calculations, can be ruled out, as the resulting pH would be around 8. Allowing to dissolve calcite and to precipitate $Fe(OH)_3$ results in the same pH of just under 8. Possible buffer candidates are feldspars and clay minerals, such as illite or smectite, the dissolution of which would result in the release of hydroxyl ions into the solution. However, the modelling only allows to bracket-in possible systems, but does not allow their positive identification.

Table 4: Possible buffer systems in pre-equilibrated Sievi granite waters and the resulting pH values for different initial iron concentrations.

Buffer system	pH for $C_{Fe} = 1.33 \cdot 10^{-3}$	pH for $C_{Fe} = 1.00 \cdot 10^{-6}$
Measured	6.64	-
$Fe(OH)_3$	3.41	5.75
Calcite	7.98	8.11
Albite	4.62	6.88
Illite	4.17	5.73
Smectite (high Fe, Mg)	6.12	7.37
$Fe(OH)_3$ + Calcite	7.98	8.11
$Fe(OH)_3$ + Albite	4.34	6.83
$Fe(OH)_3$ + Illite	3.86	5.78
$Fe(OH)_3$ + Smectite (high Fe, Mg)	6.50	7.55

Based on these preliminary calculations, it was decided to maintain equilibrium with $Fe(OH)_3$ and illite in further calculations. This intends to represent pH-buffering by fracture infills and weathering products.

5.2 Hydraulic model

During the experiment, a drop in the flow-rate after 500 hours by one half and a further drop after 2700 hours by one half again has been observed (cf. Figure 19). The resulting tracer breakthrough curves for a flow rate that has been halved is shown in Figure 11. Still rather fast breakthrough is indicated.

The calculations have been repeated with a dual-porosity model, assuming that half of the porosity (n_e= 5%) contributes to the transport and the other half constitutes an immobile reservoir. The dual-porosity model results in a significant delay of the breakthrough as can be seen by comparing Figures 11 and 12.

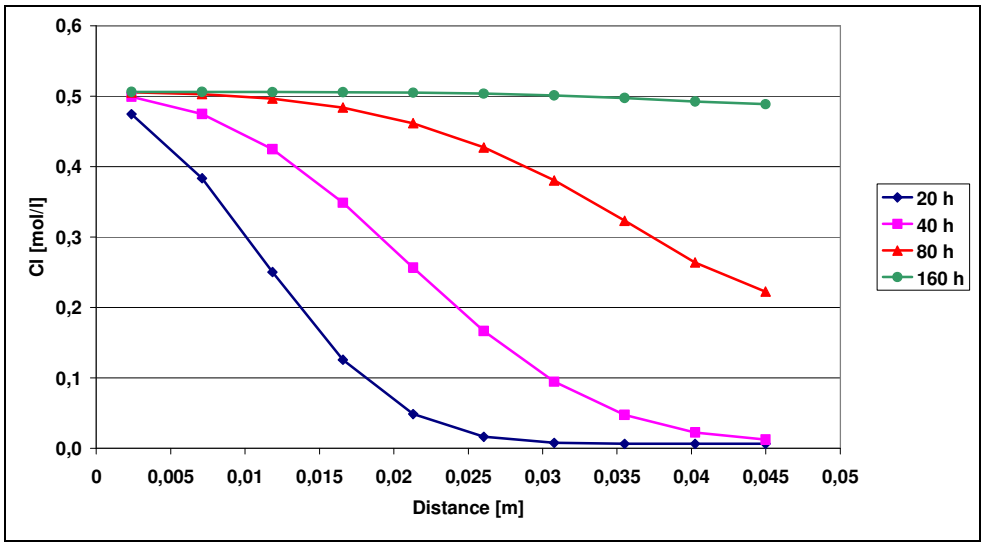

Figure 11: Tracer profiles with a flow-rate of 0.0085 cm^3/min, a dispersion length $\alpha_L = 5 \cdot 10^{-4}$ m and an effective porosity $n_{eff} = 5\%$.

5.3 Uranium migration

Using the experimental water compositions and the new hydraulic data, the uranium migration calculations have been repeated. Preliminary calculations show that schoepite is still a good proxy for an oxic solid uranium phase that controls solubility. The presence of phosphate in the waters, however, would make it not unlikely that a phase such as $(UO_2)_3(PO_4)_2 \cdot 4H_2O$ may exert influence on the solubility of uranium.

If no precipitation of schoepite was allowed, the shape of the curves by which its saturation is reached in depth is identical to the tracer profiles (Figure 13).

For the precipitation reactions various scenarios can be envisaged: 1) precipitation takes place through the porosity, regardless, whether the water in it is mobile or immobile, 2) precipitation takes place only in the immobile porosity.

For scenario 1 Figure 14 shows the resulting uranium concentration profiles, the profile of saturation with respect to schoepite and the time-profile of the effluent uranium concentration.

When precipitation is allowed only in the immobile cells, the profiles look somewhat different in the top part of the sample, but become quickly controlled by schoepite throughout the sample. Due to the absence of precipitation kinetics all the precipitation occurs in the first couple of cells.

In terms of uranium breakthrough, however, there is no difference between the two scenarios (Figure 16).

Two sample runs using $(UO_2)_3(PO_4)_2 \cdot 4H_2O$ and saleeite as controlling phases show that uranium solubility would be about the same for both minerals, but one order of magnitude higher than for schoepite (Figure 17).

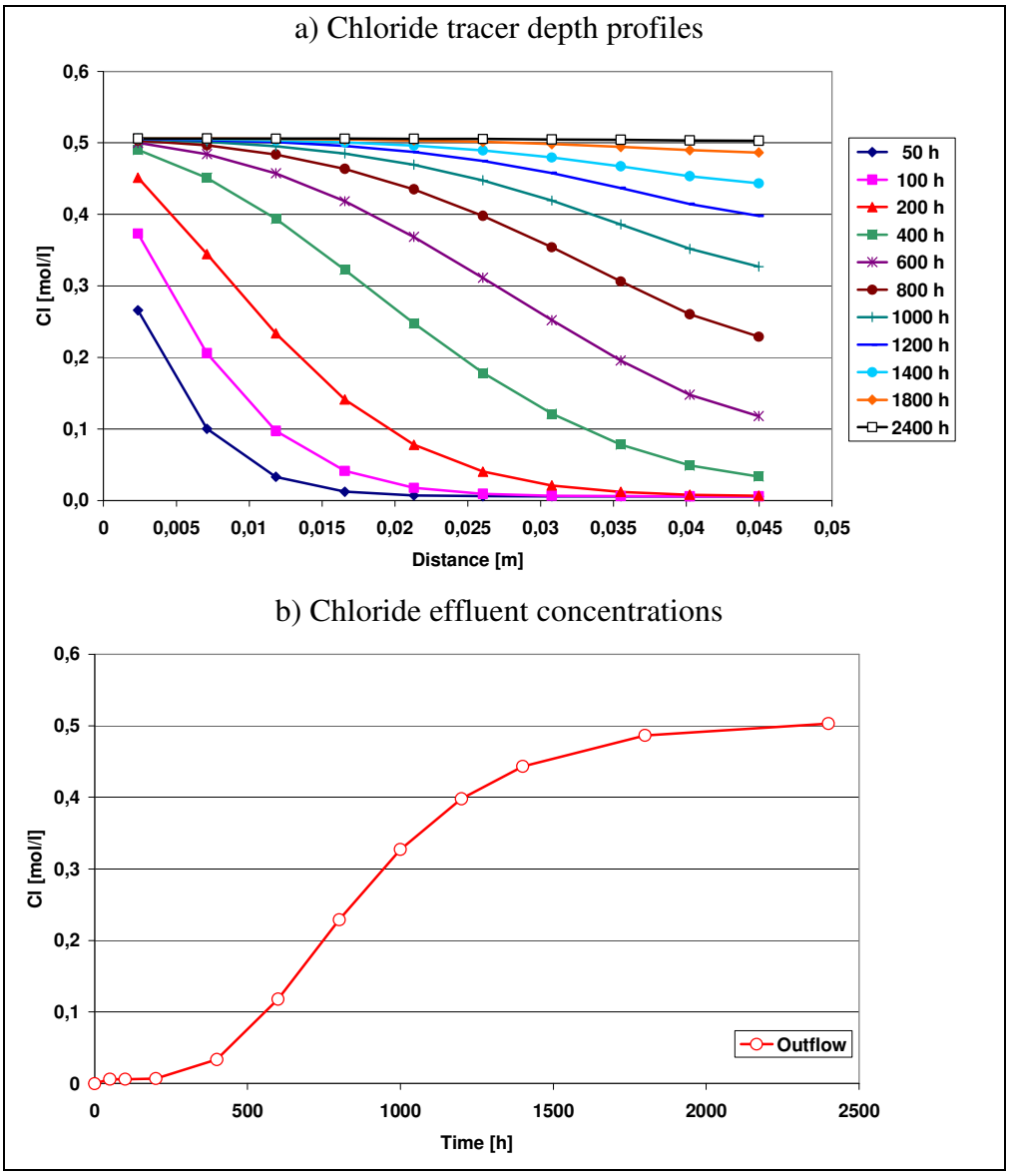

Figure 12: Tracer profiles for a dual-porosity model with the same hydraulic parameter values as in Figure 11.

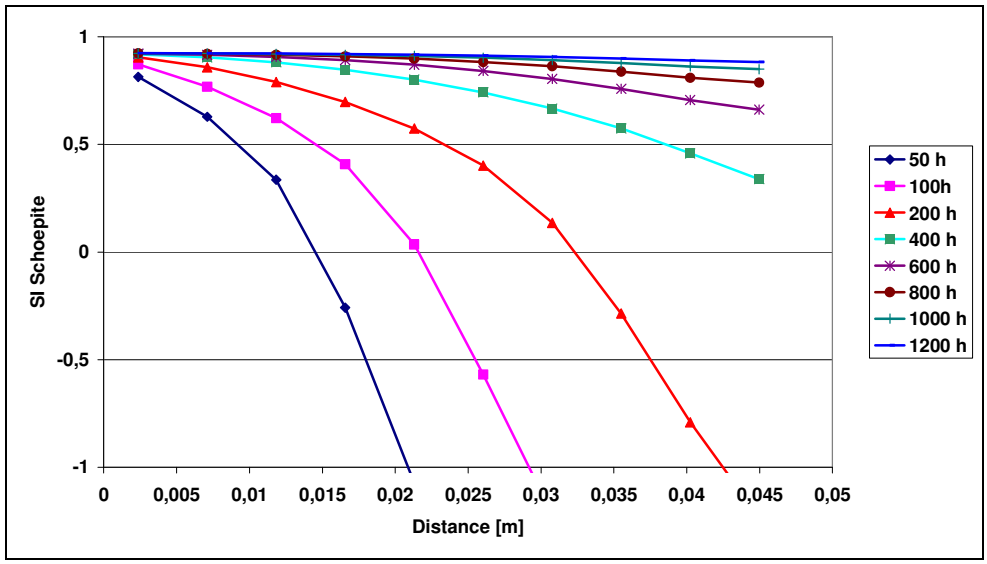

Figure 13: Depth profiles for the saturation index of schoepite. Same hydraulic parameter values as in Figure 12.

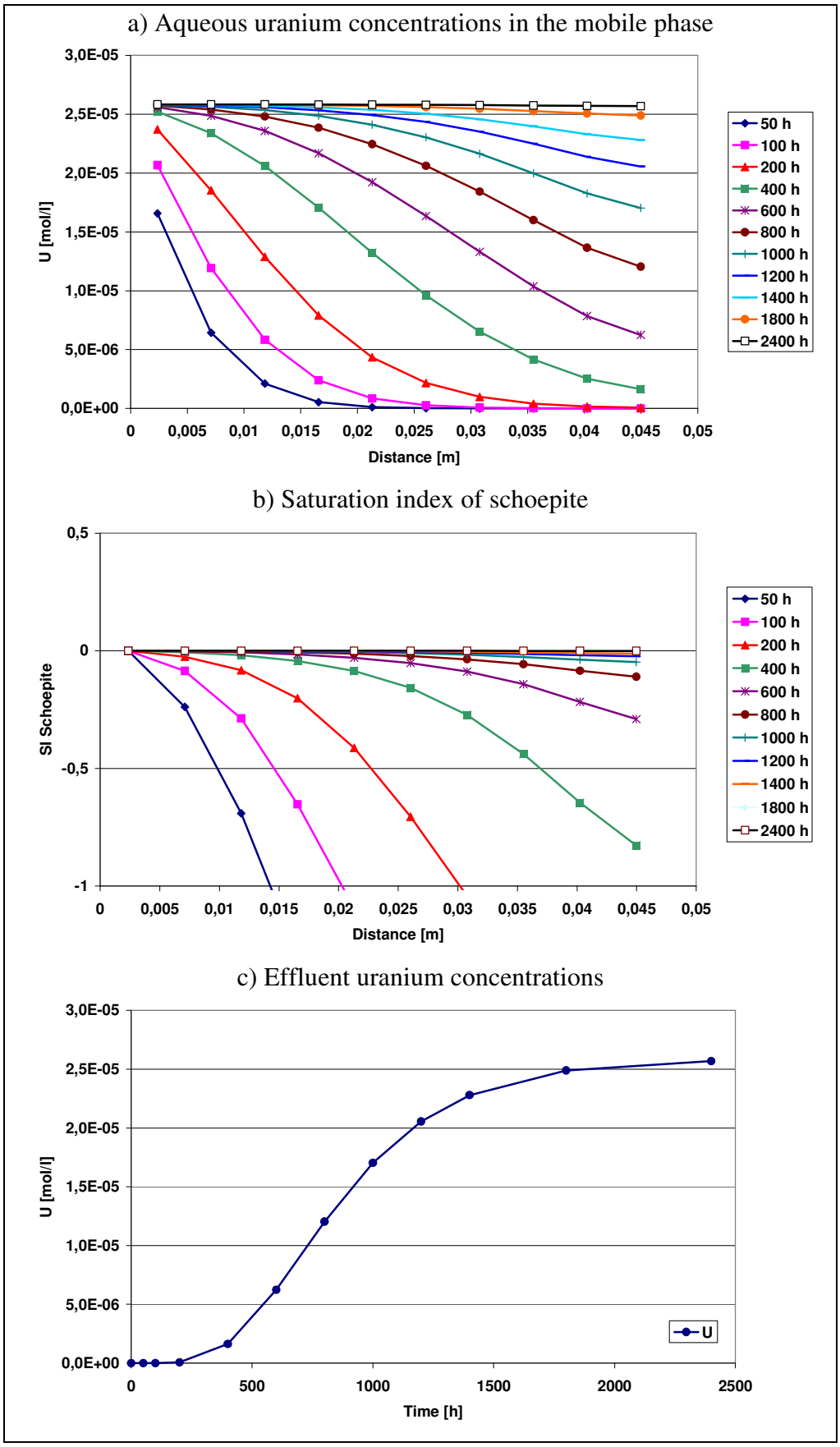

Figure 14: Flooding the core with a uranium solution of $3.176 \cdot 10^{-4}$ mol/dm^3 while allowing schoepite to precipitate in all cells. Same hydraulic parameter values as in Figure 12.

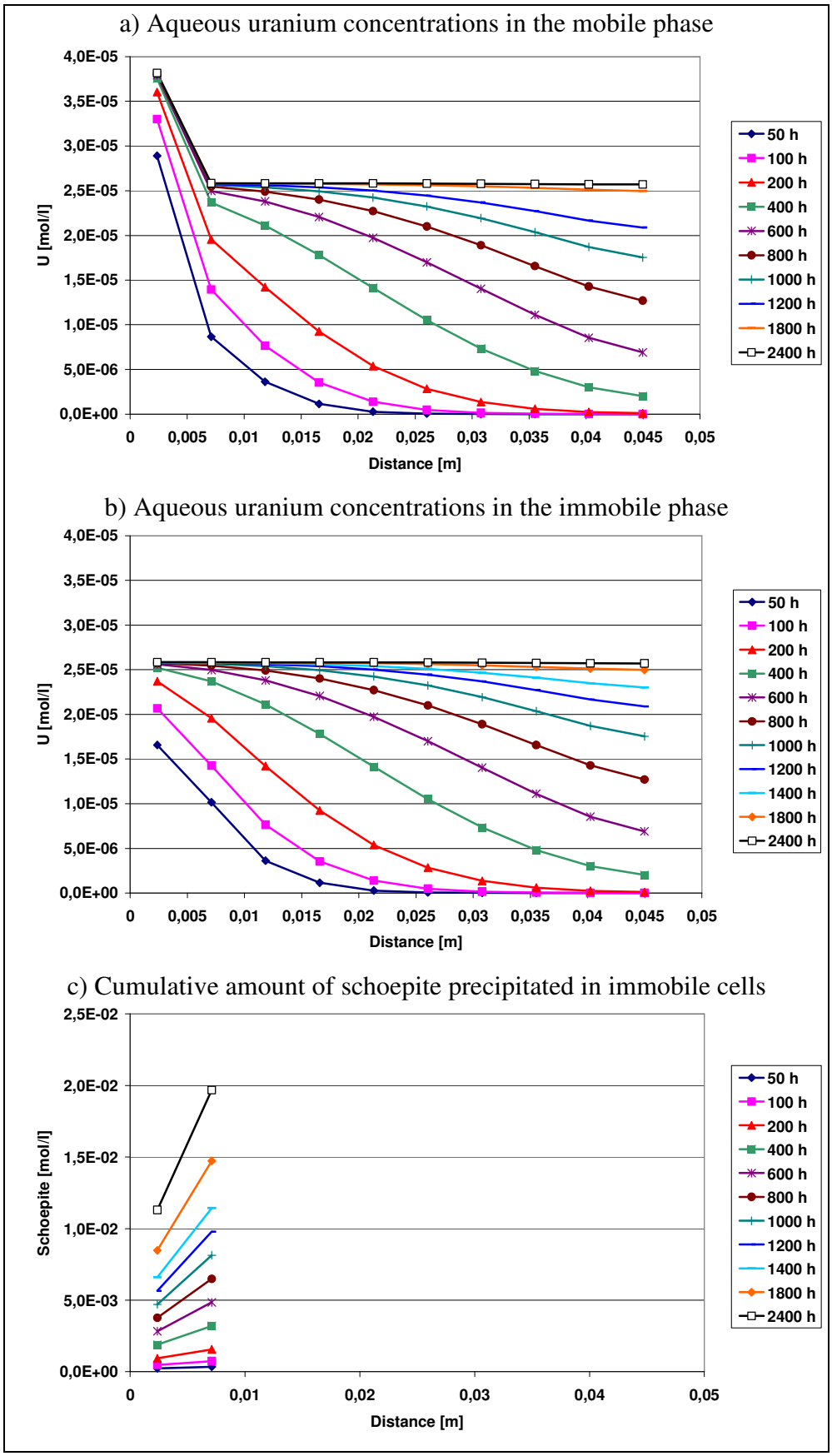

Figure 15: Flooding the core with a uranium solution of $3.176 \cdot 10^{-4}$ mol/dm^3 while allowing schoepite to precipitate in immobile cells only. Same hydraulic parameter values as in Figure 12.

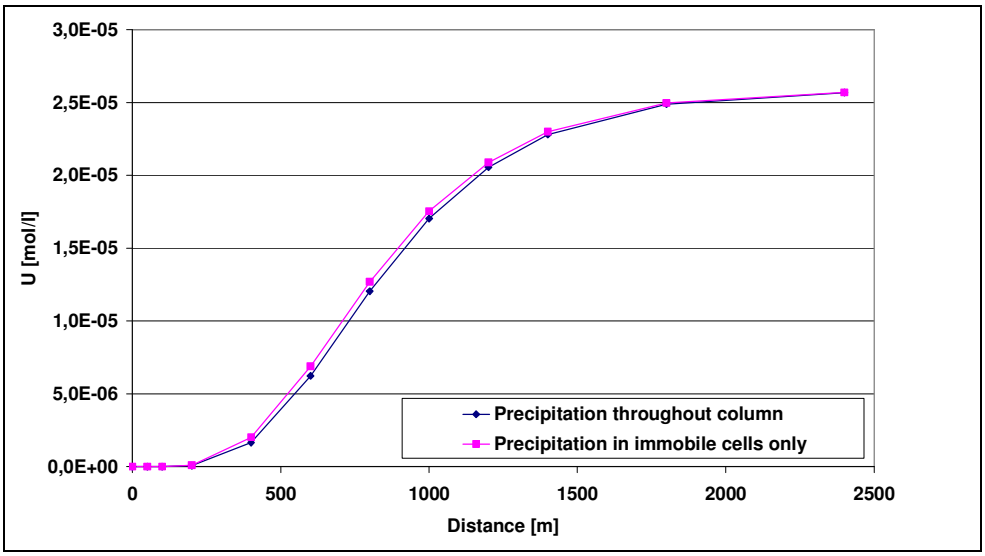

Figure 16: Comparison of breakthrough curves for different scenarios of precipitation with schoepite as controlling phase. Same hydraulic parameter values as in Figure 12.

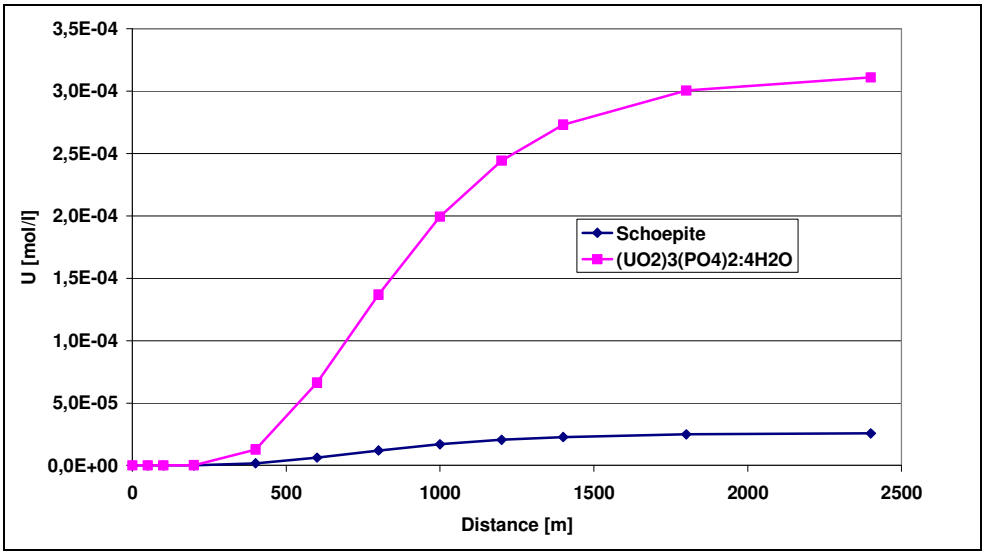

Figure 17: Comparison of breakthrough curves with schoepite and $(UO_2)_3(PO_4)_2 \cdot 4H_2O$ as solubility controlling phases. Same hydraulic parameter values as in Figure 12.

5.4 Major ion chemistry

The effluent major ion chemistry reflects the phases that have been programmed to precipitate or dissolve, namely $Fe(OH)_3$, illite and schoepite. Hence only potassium, iron, aluminium and alkalinity (carbon) show appreciable developments (Figure 18a), the concentrations converge to values that represent equilibrium with the above solid phases. The precipitation of hydroxyl-consuming phases is marked by a drop of the pH-value over time (Figure 18b).

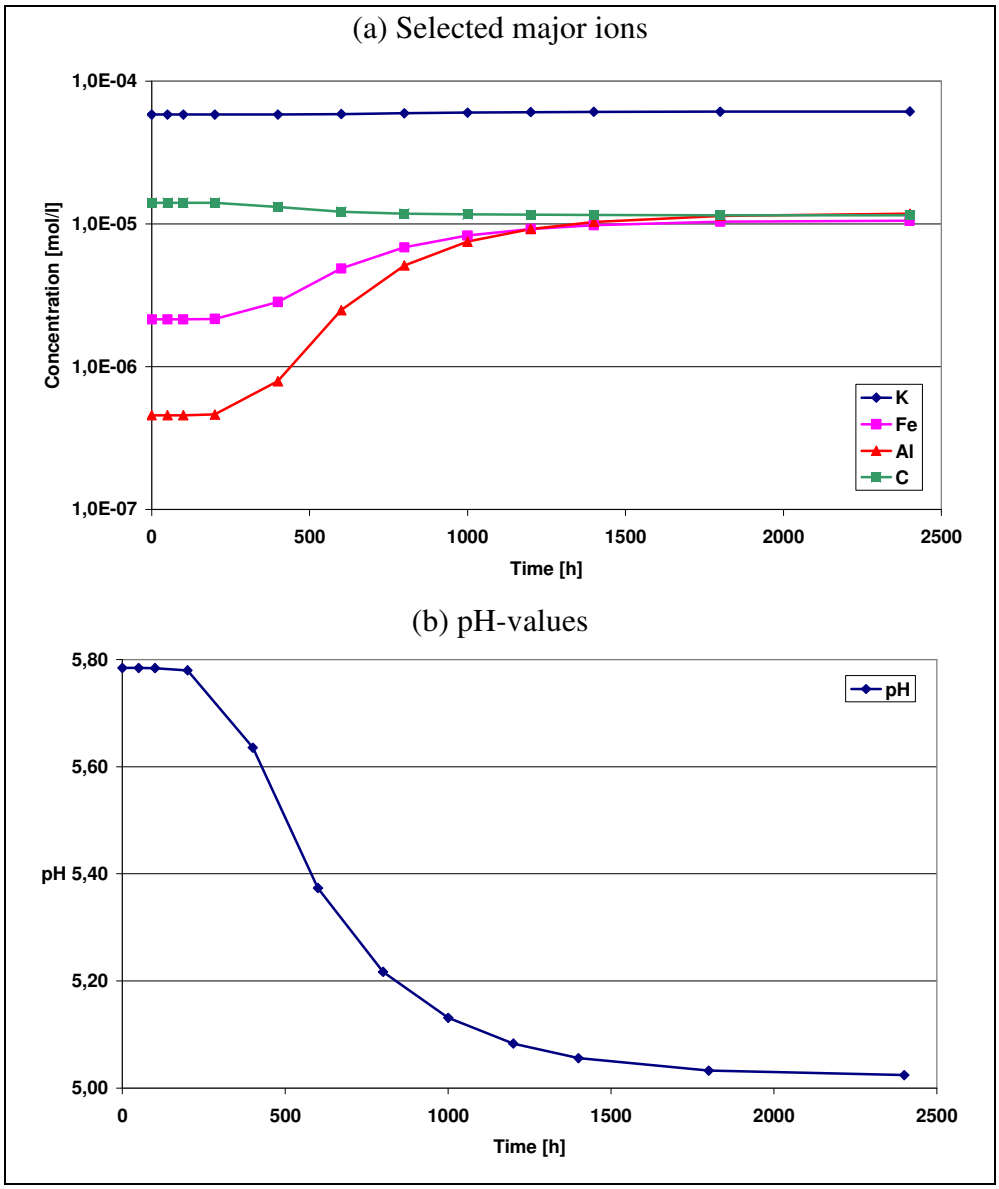

Figure 18: Major ion concentrations (a) and pH-values (b) in column effluents. Same hydraulic parameter values as in Figure 12.

6. Comparison with experimental data

6.1 Flow data

The flow rates dropped considerably during the course of the experiment and most interestingly at two distinct points in time, after 500 hours and after 2500 hours. Initially the flow rate was 1 cm^3/h as during the blank test. After 500 hours the flow rate decreased to 0.46 cm^3/h and after 2500 decreased further to 0.25 cm^3/h (Figure 19).

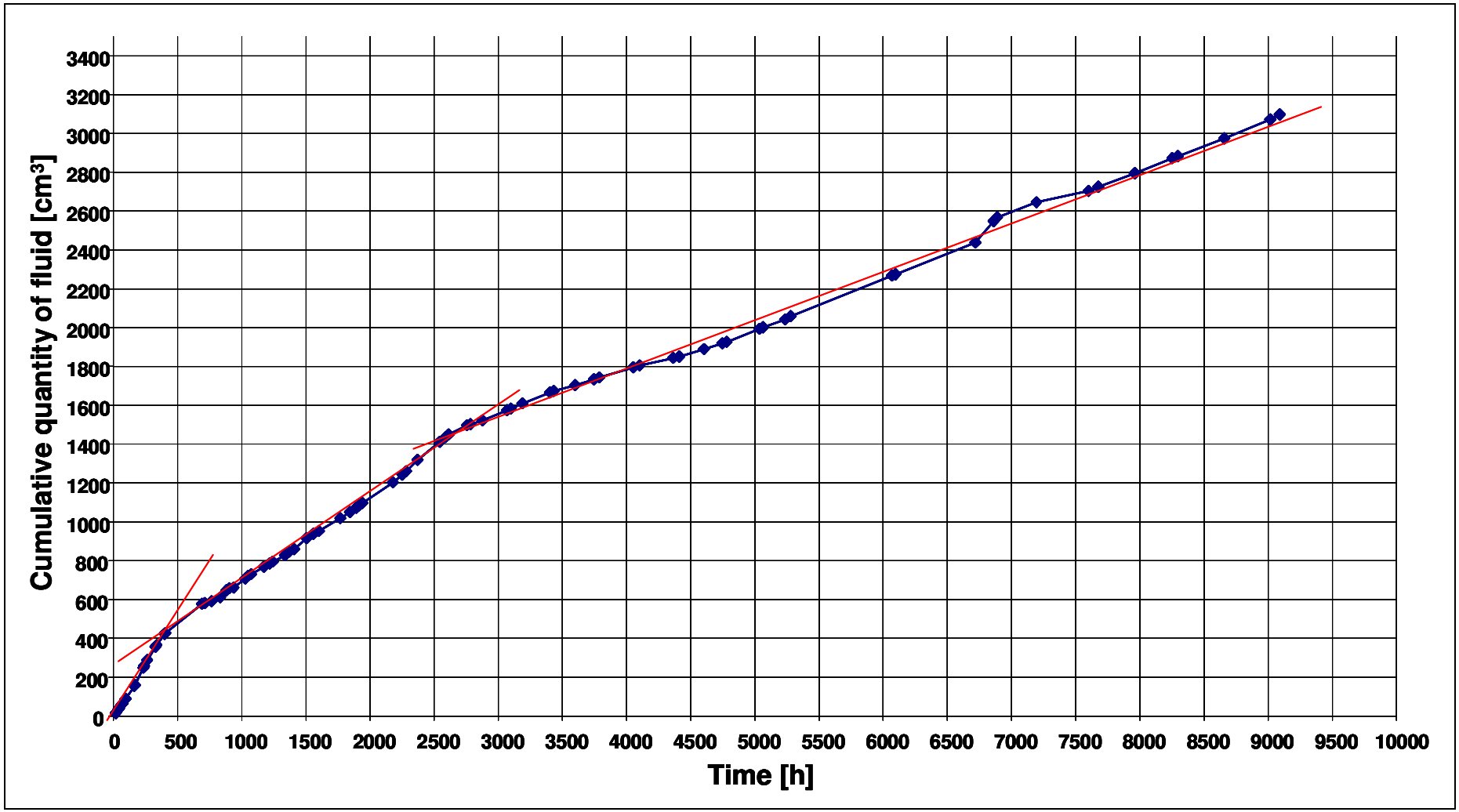

Figure 19: Measured cumulative volumes of fluid flow *vs*. time.

6.2 Effluent composition

The aqueous solution concentrations measured in the effluent of the column are graphically represented in Figure 20 and given in Table 5. A few qualitative observations help guide further modelling efforts:

— the dip at 400 hours is due to a breakdown in the pressure supply, which interrupted the experimental run; before and after the interruption the concentration of almost all constituents increase steadily, albeit at different rates;

— the outflow concentrations of measured elements indicate reactions that effect the different elements in a different way. The concentration of Ca and Mg increase to level of after 7000 hours; the concentration of Na and K increases as Ca and Mg, but drops again after 3000 hours; silica values are scattered, but appear to drop towards the end of the experiment; phosphate values go through a peak at 5000 hours and drop off afterwards; the effluent uranium concentration, to the contrary, steadily increases over the whole experimental time; neither chloride concentrations nor alkalinity was measured;

— pH does not show a very marked trend, but drops by about 0.5 units over the experimental period;

— the total increase in dissolved constituents, based on electrical conductivity, first increases by a factor of 2.47 and then drops off to a value near the original one (Table 5);

— when compared to the inflow concentrations of water pre-equilibrated with Sievi-Granodiorite (Table 3), the factors only range between one and four; which appears to indicate the presence of an initial solution in the column that has not been in equilibrium with the rock and is more dilute than the equilibrium solution;

— in order to arrive at the observed concentrations (Table 5), a solid with the hypothetical stoichiometry of $Na_1K_{0.03}Ca_{1.2}Mg_{1.1}(SO_4)_{0.06}(PO_4)_{0.002}(SiO_2)_{0.12}Sr_{0.002}Cl_{6.2}$ would need to dissolve, or alternatively several solids that together would give this stoichiometry.

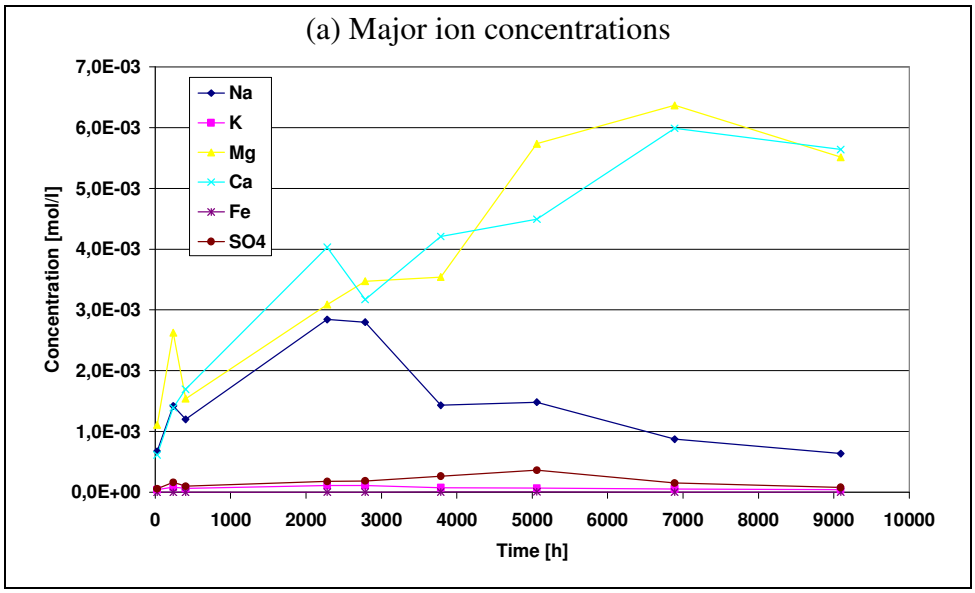

Figure 20: Evolution of measured effluent concentrations.

(b) Minor ion concentrations

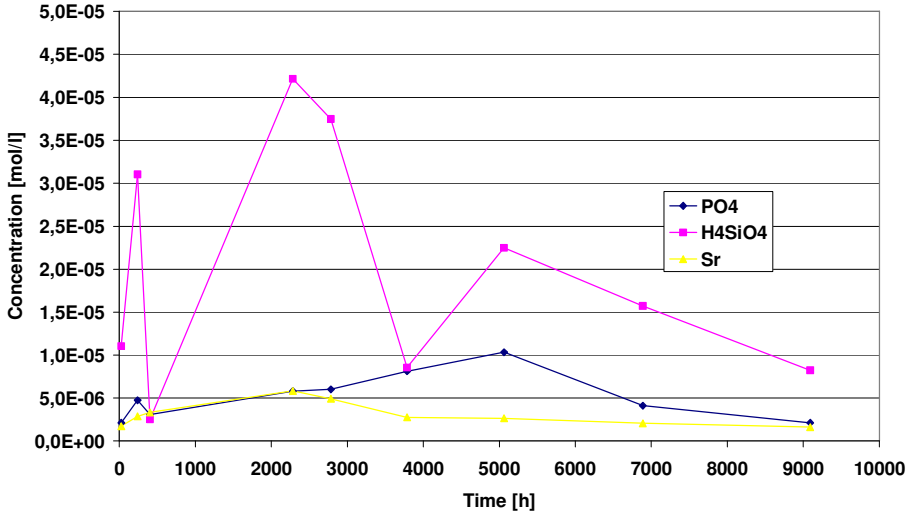

(c) Uranium concentrations

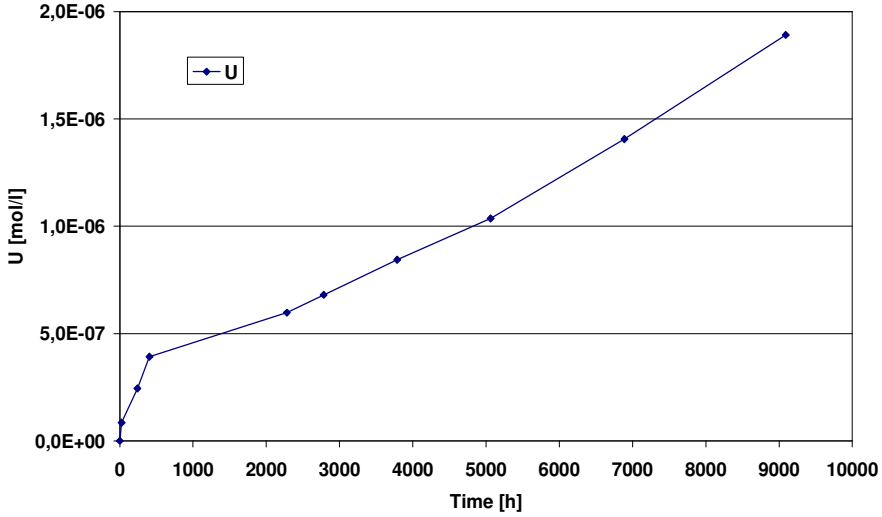

(d) pH and electrical conductivity

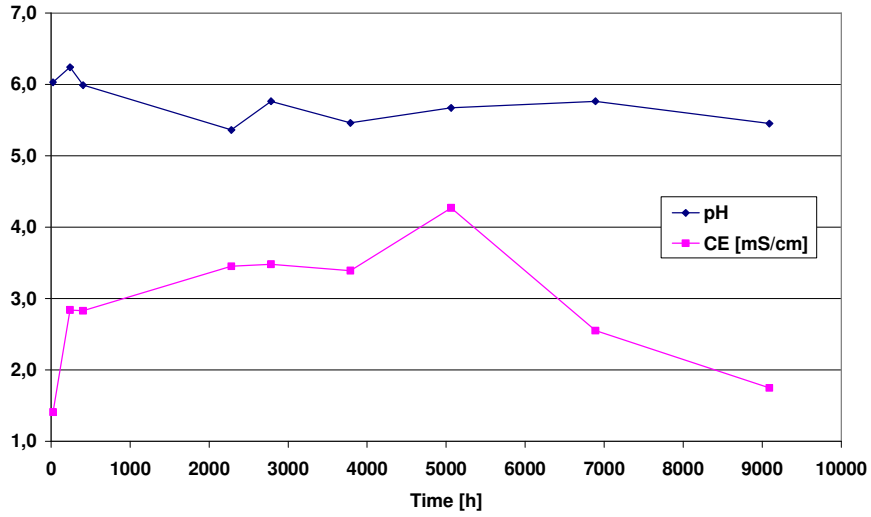

Figure 20 continued: Evolution of measured effluent concentrations.

Table 5: Measured effluent concentration [mol·dm^{-3}].

Time [h]	Na	K	Mg	Ca	Fe	SO_4
inflow	$9.270 \cdot 10^{-4}$	$5.810 \cdot 10^{-5}$	$1.670 \cdot 10^{-3}$	$8.850 \cdot 10^{-3}$	$1.330 \cdot 10^{-6}$	$0.921 \cdot 10^{-4}$
25	$6.729 \cdot 10^{-4}$	$4.118 \cdot 10^{-5}$	$1.108 \cdot 10^{-3}$	$6.165 \cdot 10^{-4}$	$5.078 \cdot 10^{-7}$	$5.809 \cdot 10^{-5}$
240	$1.423 \cdot 10^{-3}$	$8.338 \cdot 10^{-5}$	$2.628 \cdot 10^{-3}$	$1.391 \cdot 10^{-3}$	$2.555 \cdot 10^{-6}$	$1.633 \cdot 10^{-4}$
404	$1.200 \cdot 10^{-3}$	$6.624 \cdot 10^{-5}$	$1.540 \cdot 10^{-3}$	$1.696 \cdot 10^{-3}$	$1.158 \cdot 10^{-6}$	$9.869 \cdot 10^{-5}$
2281	$2.844 \cdot 10^{-3}$	$1.084 \cdot 10^{-4}$	$3.088 \cdot 10^{-3}$	$4.032 \cdot 10^{-3}$	$1.500 \cdot 10^{-6}$	$1.783 \cdot 10^{-4}$
2784	$2.800 \cdot 10^{-3}$	$1.092 \cdot 10^{-4}$	$3.473 \cdot 10^{-3}$	$3.174 \cdot 10^{-3}$	$1.458 \cdot 10^{-6}$	$1.880 \cdot 10^{-4}$
3787	$1{,}431 \cdot 10^{-3}$	$7.494 \cdot 10^{-5}$	$3.540 \cdot 10^{-3}$	$4.209 \cdot 10^{-3}$	$6.486 \cdot 10^{-6}$	$2.658 \cdot 10^{-4}$
5063	$1.482 \cdot 10^{-3}$	$6.880 \cdot 10^{-5}$	$5.735 \cdot 10^{-3}$	$4.494 \cdot 10^{-3}$	$8.998 \cdot 10^{-6}$	$3.636 \cdot 10^{-4}$
6888	$8.742 \cdot 10^{-4}$	$5.499 \cdot 10^{-5}$	$6.365 \cdot 10^{-3}$	$5.988 \cdot 10^{-3}$	$3.470 \cdot 10^{-6}$	$1.525 \cdot 10^{-4}$
9090	$6.362 \cdot 10^{-4}$	$4.271 \cdot 10^{-5}$	$5.513 \cdot 10^{-3}$	$5.639 \cdot 10^{-3}$	$3.212 \cdot 10^{-6}$	$8.016 \cdot 10^{-5}$
d_{2784} / d_0	3.02	1.88	2.08	3.59	1.10	2.06
d_{2784} / d_{25}	4.16	2.65	3.13	5.15	2.87	3.24
Time [h]	**PO_4**	**H_4SiO_4**	**Sr**	**^{238}U**	**pH**	**CE [mS/cm]**
inflow	$3.130 \cdot 10^{-6}$	$2.750 \cdot 10^{-5}$	n/a	$8.446 \cdot 10^{-8}$	6.64	n/a
25	$2.106 \cdot 10^{-6}$	$1.103 \cdot 10^{-5}$	$1.712 \cdot 10^{-6}$	$2.442 \cdot 10^{-7}$	6.03	1.41
240	$4.738 \cdot 10^{-6}$	$3.100 \cdot 10^{-5}$	$2.853 \cdot 10^{-6}$	$3.915 \cdot 10^{-7}$	6.24	2.84
404	$3.054 \cdot 10^{-6}$	$2.497 \cdot 10^{-6}$	$3.310 \cdot 10^{-6}$	$5.969 \cdot 10^{-7}$	5.99	2.83
2281	$5.791 \cdot 10^{-6}$	$4.214 \cdot 10^{-5}$	$5.821 \cdot 10^{-6}$	$6.802 \cdot 10^{-7}$	5.36	3.45
2784	$6.002 \cdot 10^{-6}$	$3.746 \cdot 10^{-5}$	$4.908 \cdot 10^{-6}$	$8.434 \cdot 10^{-7}$	5.76	3.48
3787	$8.108 \cdot 10^{-6}$	$8.531 \cdot 10^{-6}$	$2.739 \cdot 10^{-6}$	$8.434 \cdot 10^{-7}$	5.46	3.39
5063	$1.032 \cdot 10^{-5}$	$2.247 \cdot 10^{-5}$	$2.625 \cdot 10^{-6}$	$1.036 \cdot 10^{-6}$	5.67	4.27
6888	$4.107 \cdot 10^{-6}$	$1.571 \cdot 10^{-5}$	$2.054 \cdot 10^{-6}$	$1.406 \cdot 10^{-6}$	5.76	2.55
9090	$2.106 \cdot 10^{-6}$	$8.219 \cdot 10^{-6}$	$1.598 \cdot 10^{-6}$	$1.891 \cdot 10^{-6}$	5.45	1.75
d_{2784} / d_0	1.92	1.36	n/a			n/a
d_{2784} / d_{25}	2.85	3.40	2.87			2.47

Note: d_{2784} / d_0 and d_{2784} / d_{25} denote the ratios between the concentration peak and inflowing concentration and initial porewater concentrations respectively.

6.3 Static PHREEQC simulations using the experimental data

The experimentally determined water compositions from Table 5 were subject to static speciation and solubility calculations with PHREEQC and the LLNL-database. The purpose was to identify possible solubility controlling phases for major ions and for uranium.

The solutions were supersatured with respect to two uranium phases nearly throughout the whole experimental time (Figure 21), namely $(UO_2)_3(PO_4)_2 \cdot 4H_2O$ and soddyite, $(UO_2)_2SiO_4 \cdot 4H_2O$. Saturation with respect to β-$UO_{2.3333}$ was reached at the end of the experiments. These minerals were used to constrain solubilities in subsequent transport calculations.

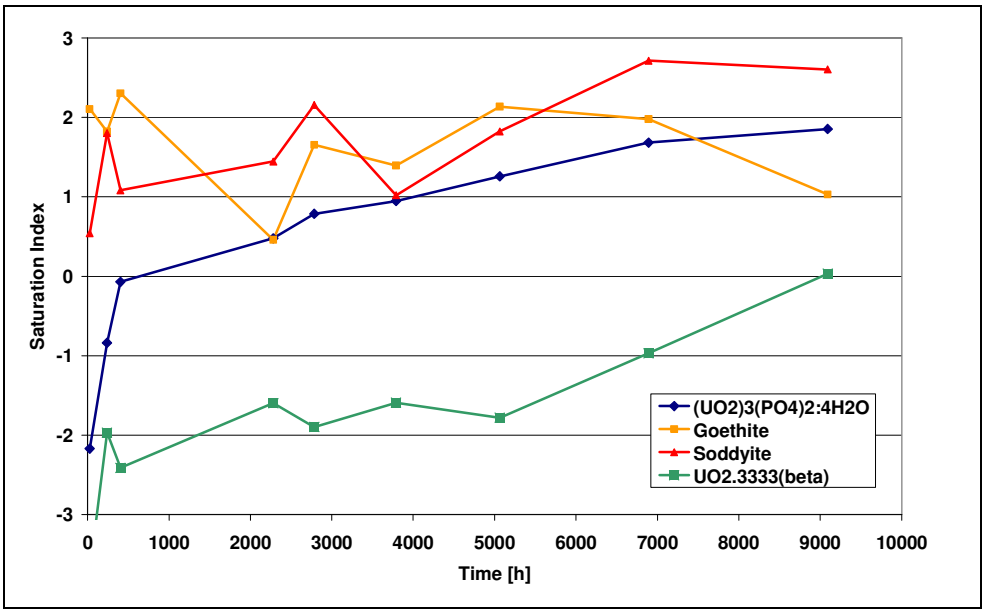

Figure 21: Calculated saturation with respect to $(UO_2)_3(PO_4)_2 \cdot 4H_2O$, soddyite and β-$UO_{2.3333}$ for experimental effluent compositions. Goethite is shown for comparison.

6.4 Reactive transport simulations

It was attempted to reproduce the measured outflow concentrations by PHREEQC reactive transport calculations, taking into account the changing flow rates over the experimental time. This required to subdivide the transport steps into three consecutive calculations using the flow-rates given in Section 6.1.

It was found that the model set up in PHREEQC was not particularly sensitive to the changing flow rates. Other parameters, in particular the assumed uranium release rate and the assumed dissolution rate of the solid matrix appear to be more important. With the absence of a tracer case, however, it is not possible to deconvolute the effects of reaction kinetics and flow rate with a view to arrive at an unique solution of the transport model.

Table 6: Mineral composition [%] of Sievi-granodiorite from drill core SY-KR7 (LINDBERG & PAANANEN, 1992).

Depth	87.7 m
Facies	Micagneiss
Plagioclase	58.2
Quartz	23.8
Biotite	13.8
Sericite	1.6
Epidote	0.2
Chlorite	1.4
Carbonates	0.2
Apatite	0.4
Opaques	0.4

The measured concentration profiles *vs.* time of the major ions (Figure 20) indicate that dissolution reactions of the rock matrix or fracture infills must take place. The main constituents of granodiorite are typically plagioclase, K-feldspar, biotite and hornblende in addition to quartz (Table 6). Typical geochemical reactions in such system are the chloritisation of hornblende, illitisation of feldspars, or the dissolution of any pre-existing weathering products. Modelling weathering/dissolution reactions, i.e. equilibration of the waters with some of these minerals (with the exception of plagioclase and biotite, for which no data were available in the LLNL-database), leads to a significant rise in system pH, as opposed to the slight dip actually observed. If such processes occurred in the experiment, it must have been balanced by some buffering reaction, for instance the precipitation of a solid phase containing hydroxyl ions, including uranyl hydroxides. However, a side effect of such buffering reactions would be the removal of cations from the solution, while in the experiment a concentration increase was observed. A pH-dip would also be observed following the oxidation of, for instance, metal sulfides, such as pyrite. Pyrite oxidation in principle could also account for the observed increase in sulfate concentrations. If the respective amounts of pyrite-derived sulfate was produced, this would result in too low pH values in the absence of an effective buffer system, for instance carbonate minerals.

A model based on instantaneous equilibration with selected minerals leads to a steep rise of major ion concentrations ending in a concentration plateau that is controlled by the respective solubility products (Figs. 22ff). The observed concentration *vs*. time profiles can only be accounted for by assuming some sort of dissolution kinetics. The unavailability of dispersion data from a tracer test and of independently determined kinetic data meant that these two effects cannot be separated and that any calculation models will not be unique. This is a drawback of all subsequent model calculations.

In order to account for the concentration increase of major ions, initially an arbitrary reaction was defined that added ions according to the stoichiometry $Na_1K_{0.03}Ca_{3.6}Mg_{3.3}(SO_4)_{0.06}(PO_4)_{0.01}(SiO_2)_{0.1}Sr_{0.01}Cl_{6.2}$. The chloride value was derived from the ionic balance (Table 5) and in subsequent calculations adjusted to the desired target pH, which was the measured final effluent pH. A value of $2.81 \cdot 10^{-5}$ mol was chosen as arbitrary reaction rate per time step based on preliminary calculations by trial-and-error to arrive at the measured concentrations as target concentrations.

The lack of data for some major anions, particularly carbonate and chloride, adds to the difficulty of constraining the model. Various parameter value combinations were tried out in order to get a handle on those parameters not measured. Assumptions for realistic scenarios include:

- the inflowing solution is in equilibrium with ambient CO_2 and/or O_2 partial pressures and/or
- the triaxial cell is in equilibrium with ambient CO_2 and/or O_2 partial pressures

Initial runs maintaining equilibrium with ambient CO_2 partial pressures were found to push pH-values too high, if all the missing anions were assumed to be carbonate. Therefore, a certain amount of the ionic balance must be made up by another anion. By trial and error more and more chloride was added to the model until the measured pH was reached, while total carbonate concentrations were let to float in order to balance the overall charge in the system.

In order to better understand the system behaviour, it is very helpful to ponder about the possible driving forces behind the observed bulk changes. First of all, although the inflowing solution was pre-equilibrated water, as this water was in equilibrium with crushed rock, it may have been exposed to a somewhat different relative mineral composition. On the other hand, the major ‘foreign’ component in the system was the depleted uranium disc and its corrosion constitutes a significant driving force for geochemical changes downstream.

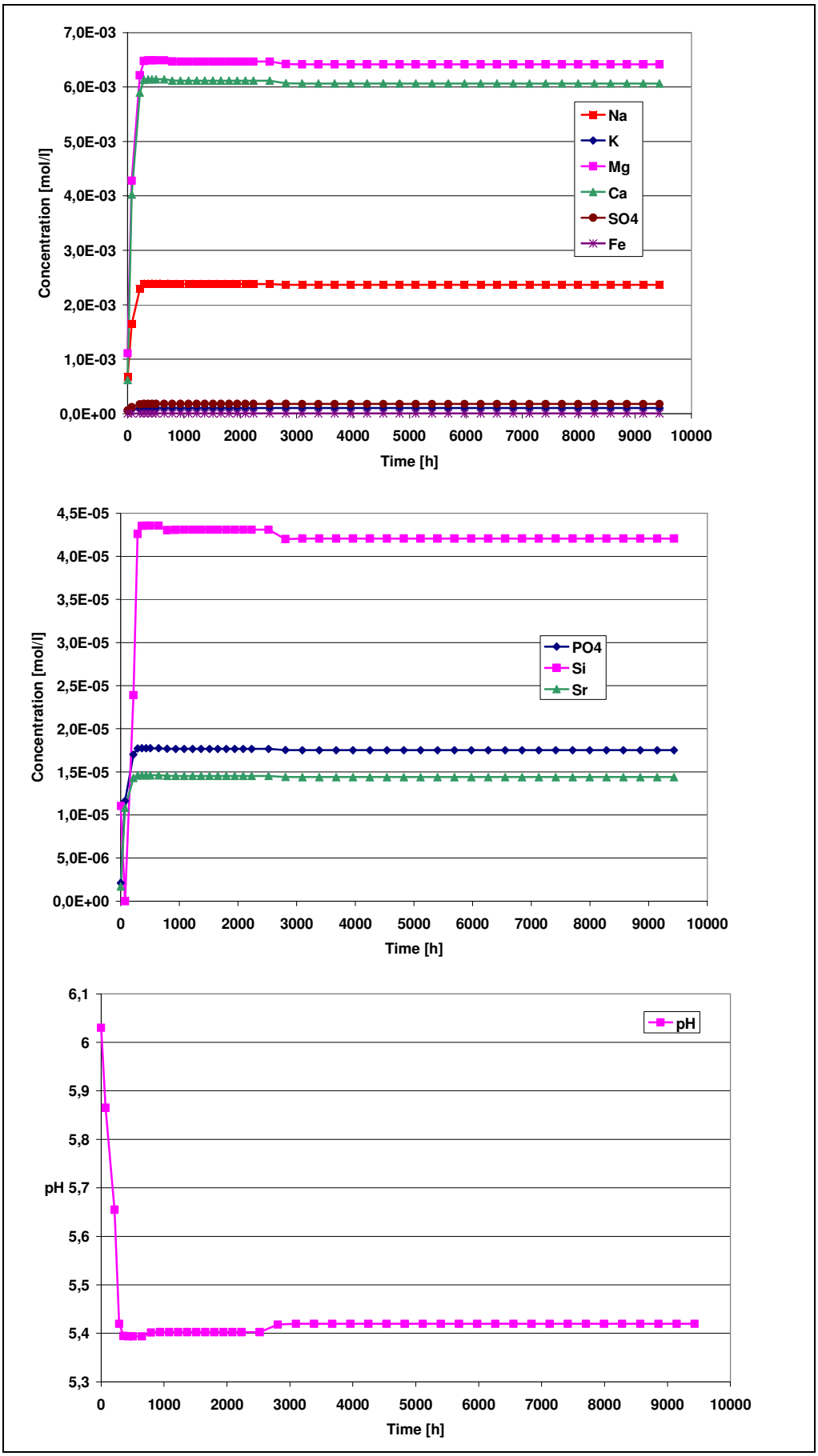

Figure 22: Calculated effluent concentrations and pH for a model with U-solubility control by Soddyite.

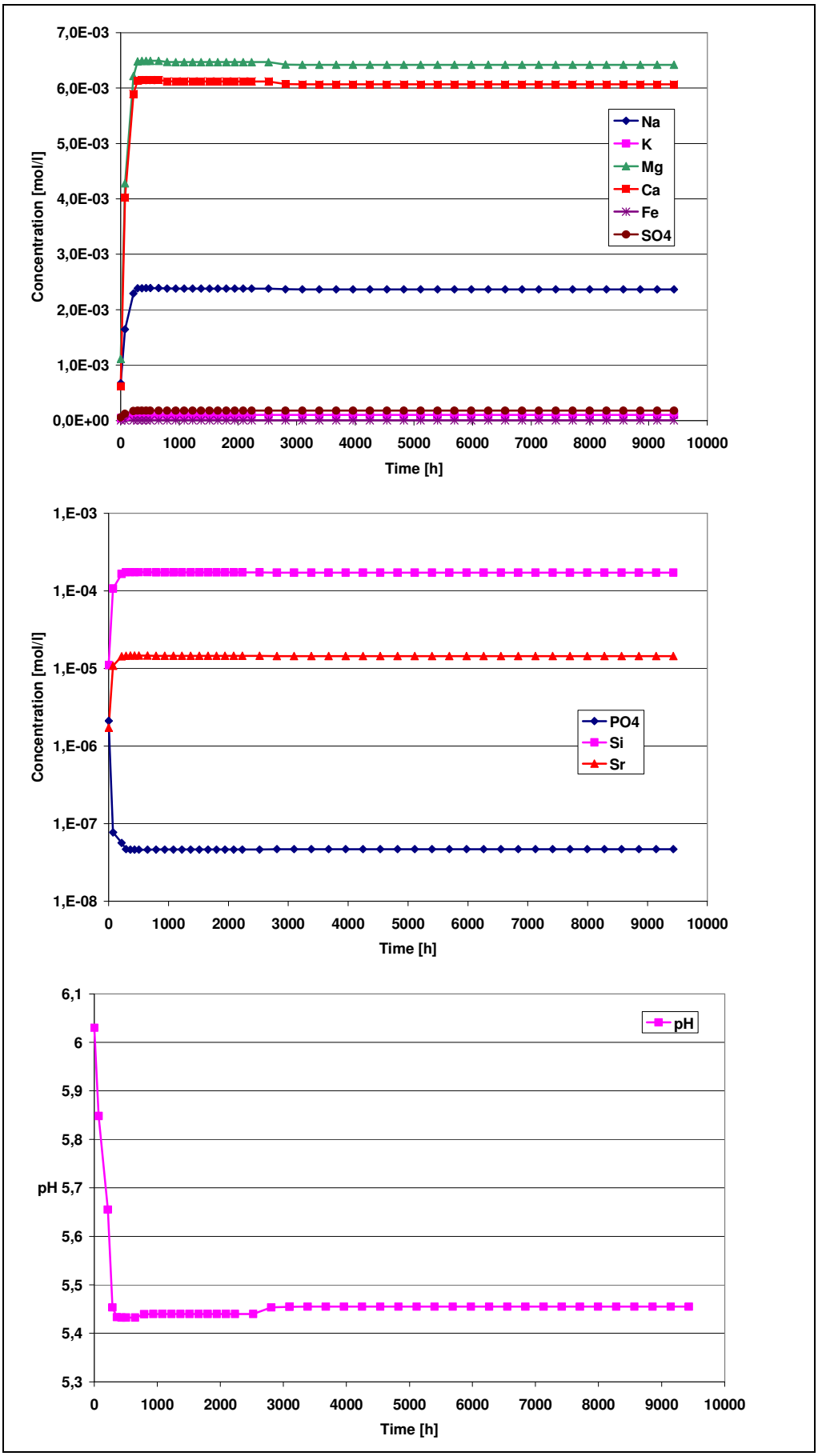

Figure 23: Calculated effluent concentrations and pH for a model with U-solubility control by $(UO_2)_3(PO_4)_2 \cdot 4H_2O$.

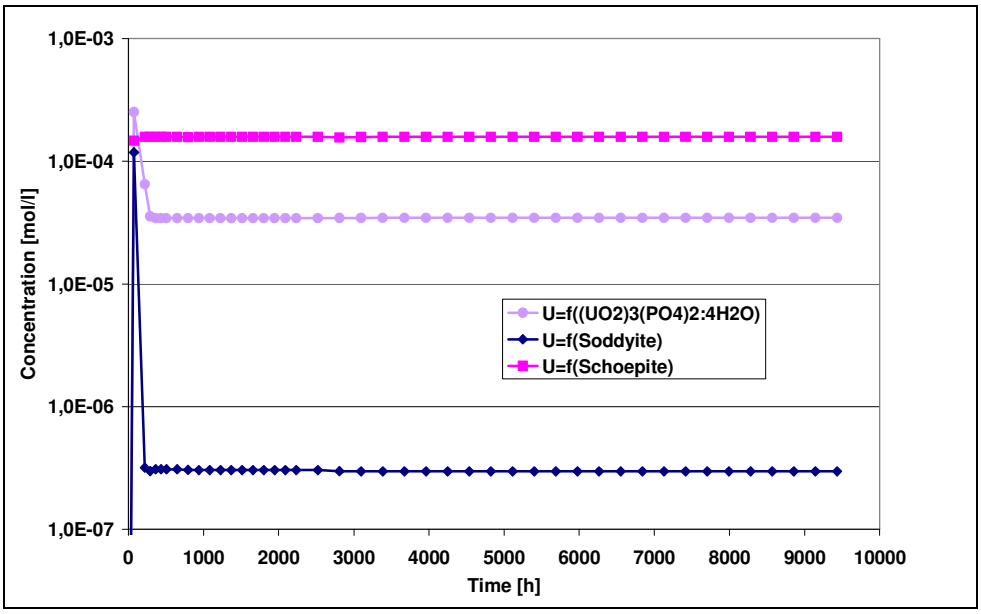

Figure 24: Calculated effluent uranium concentrations for different solubility controlling phases.

In the absence of strong pH buffering, the release and precipitation of uranium could change the system pH significantly due to e.g. removal of hydroxyl ions from solution. This is what happened in static modelling runs. In transport modelling runs, due to the lack of precipitation kinetics, precipitation happens only in the cell where the supersaturation is calculated and any pH changes are 'smeared' out by diffusion/dispersion effects and thus made less pronounced.

Figure 22 and 23 show the calculated evolution of the major ion chemistry as a function of the precipitating uranium phase. As expected, both variants show only differences for the ions that are actually involved in the respective precipitation reaction.

Again the instant precipitation implied by an equilibrium model has the effect that models using different solid phases for solubility control only differ in the level of the final uranium concentration, but not fundamentally in the time vs. concentration profile (Figure 24). Comparing the calculated uranium concentration for different solubility controlling phases (Figure 24) with the measured uranium concentrations (Figure 20c) indicates a considerable level of conservatism in the calculations. Calculated final uranium concentrations for schoepite, $(UO_2)_8O_2(OH)_{12}\cdot 12(H_2O)$, and $(UO_2)_3(PO_4)_2\cdot 4H_2O$ are two orders of magnitude above the measured ones, while those for soddyite, $(UO_2)_2SiO_4\cdot 2(H_2O)$, are at the same level. The observed steady increase in uranium effluent concentration up to 9090 hours (375 days) could not be reproduced with the current model. The likely cause is the lack of precipitation kinetics. Unfortunately the experiment had to be terminated before a possible solubility controlled plateau concentration of uranium could was attained.

7. Summary and Conclusions

The present report summarises efforts to develop a model for uranium migration in hardrocks. Akin to the situation faced by a developing deep disposal programme, the modelling efforts started out with a minimum of initial information. This forced to take the approach of blind predictions. Blind predictions initially utilise generic information for building a conceptual model. This conceptual model is subsequently refined using site-specific information as it becomes available. At the same time the blind predictions are used to drive the experimental programme, as they help to identify data needs and data gaps.

Only the geometry of the experimental set-up, the rock type (granodiorite) and the initial flow rate were known in the first instance. Generic data for granite/granodiorite pore waters were used to scope the conceptual model. These data, together with standard thermodynamic data compilations, allowed potential solubility controlling phases to be identified. By varying the parameters for variant hydraulic models it was then possible to obtain preliminary estimates of mass transfer. Comparison with early effluent data showed that the choice of a dual-porosity model was appropriate. However, these model calculations also showed that the model could not be adequately constrained in the absence of tracer tests. Thus, the parameter values for dispersion lengths, effective porosity and the choice of single or dual porosity can be manipulated in order to arrive at similar overall model solutions. This lack of uniqueness becomes even more apparent when reactive transport calculations are undertaken, where heterogeneous reactions rates are additional variables. Confidence ascribed to retrospective fitting is often overstated and should always be viewed in the context of degrees of freedom; it does not constitute 'model validation.'

The experiment demonstrated that uranium can migrate over very short timescales, at appreciable concentrations; a fact not predicted by the majority of model approaches. In turn, the calculations highlight that incomplete system-specific knowledge, which would be much more acute in field situations, may have to be compensated for by unrealistic assumptions regarding system behaviour. The normal response in safety assessments is to adopt parameter values for the chosen (usually equilibrium) model that are deemed overly conservative. These results show that they may or may not be conservative in terms of contaminant transport depending on how well they represent the system.

A detailed knowledge of the mineral phases present, which must also include accessory minerals, is essential in order to construct meaningful geochemical transport models. Many inter-related dissolution and precipitation reactions may occur simultaneously and it is, therefore, impossible to arrive at a unique solution with input and output concentrations alone. In the present case, an assessment of the secondary uranium phases on the surface of the dissolving uranium disc and within the column respectively, will allow a mass balance to be constructed. This is obviously more difficult with field investigations, although an understanding of secondary uranium phase formation permits defensible conclusions to be drawn on the effectiveness of host rock retardation.

9. References

BAUMANN, N., ARNOLD, T, GEIPEL, G, TRUEMAN, E, BLACK, S, READ, D. (2006). Detection of U(VI) on the surface of altered depleted uranium by TRLFS.- Sci.. Tot Env. **366**: 905-909.

BRUNO, J., ARCOS, D., DURO, L. (1999): Processes and features affecting the near field hydrochemistry. Groundwater-Bentonite interaction.- SKB Technical Report TR-99-29, 56 p.

FINCH, R.J., COOPER, M.A., HAWTHORNE, F.C., EWING, R.C. (1996): The Crystal Structure of Schoepite $[(UO_2)_8O_2(OH)_{12}](H_2O)_{12}$.- The Canadian Mineralogist **34**: 1071-1088.

JANG, J.-H., DEMPSEY, B.A., BURGOS, W.D. (2006): Solubility of Schoepite: Comparison and selection of complexation constants for U(VI).- Water Research **40**(14): 2738-2746.

LINDBERG, A., PAANANEN, M. (1992): Konginkankaan kivetyn, Sievin syyryn ja eurajoen Olkiluodon kallionäytteiden petrografia, geokemia ja geofysiika kairanreiät KI-KR7, SY-KR7 ja OL-KR6.- TVO/Paikkatutkimukset Työraportti 92-34, Toukokuu.

OSTANIN, S., ZELLER, P. (2007): *Ab initio* study of the uranyl oxide hydrates: a proton transfer mediated by water.- J. Phys.: Condens. Matter **19**(246108): 12pp.

PAYNE, T.E., EDIS, A.R., FENTON, B.R., WAITE, T.D. (2001): Comparison of laboratory uranium sorption data with 'in situ distribution coefficients' at the Koongarra uranium deposit, Northern Australia.- J. Environm. Radioactivity **57**(1): 35-55.

PARKHURST, D.L., APPELO, C.A.J. (1999): User's guide to PHREEQC--A computer program for speciation, batch-reaction, one-dimensional transport, and inverse geochemical calculations.- U.S. Geological Survey Water-Resources Investigations Report 99-4259.

READ, D. (1991) CHEMVAL Project: Testing of coupled chemical transport models.- CEC Report EUR13675EN.

REGENSPURG, S., SCHÄFER, T., SCHILD, D., MALMSTRÖM, M.E. (2007): Uranium(VI) Sorption and Reduction by Granitic Minerals in Bicarbonate Solutions.- MIGRATION '07, 11th International Conference on the Chemistry and Migration Behaviour of Actinides and Fission Products in the Geosphere, Abstract PA3-29: 196.

SHAW, S., BAXTER, A.C., JACKMAN, S.A., THOMPSON, I.P. (2007): Geochemical and microbiological controls on the corrosion and transport of depleted uranium in soil.- Goldschmidt Conference Abstracts, **A925**: http://www.the-conference.com/2007/gold2007/abstracts/A925.pdf

SIDBORN, M. (2007): Modelling Long-Term Redox Processes and Oxygen Scavenging in Fractured Crystalline Rocks.- PhD Thesis, KTH School of Chemical Science and Engineering, TRITA-CHE-Report 2007-60: 89 p., Stockholm, Sweden.

SIDBORN, M., NERETNIEKS, I. (2007): Modelling Oxygen Scavenging in Granitic Rocks: Glaciation Implications.- MIGRATION '07, 11th International Conference on the Chemistry and Migration Behaviour of Actinides and Fission Products in the Geosphere, Abstract PC3-6: 246.

SVENSK KÄRNBRÄNSLEHANTERING AB (2006): Long-term safety for KBS-3 repositories at Forsmark and Laxemar - a first evaluation. Main report of the SR-Can project.- Report SKB TR-06-09: 613 p.

SYLWESTER, E. R., HUDSON, E.A., ALLEN, P.G. (2000): The structure of uranium (VI) sorption complexes on silica, alumina, and montmorillonite.- Geochim. Cosmochim. Acta **64**(14): 2431-2438.

TRUEMAN, E, BLACK, S, READ, D. (2004) Characterisation of depleted uranium (DU) from an unfired CHARM-3 penetrator.- Sci. Tot. Env. **327**, 337-340.

TRUEMAN, E, BLACK, S, READ, D., HODSON, M. (2003). Alteration of depleted uranium metal.- Geochim. Cosmochim. Acta, **67**: A493.

WAITE, T.D., DAVIS, J.A., PAYNE, T.E., WAYCHUNAS, G.A., XU, N. (1994): Uranium(VI) Adsorption to Ferrihydrite: Application of a Surface Complexation Model.- Geochim. Cosmochim. Acta **58**(24): 5465-5478.

European Commission

EUR 23816 EN – Joint Research Centre – Institute for Energy
Title: Uranium Migration in Crystalline Rocks
Author(s): W.E. Falck, D. Read, S. Black, D. Thornley, M. Siitari-Kauppi
Luxembourg: Office for Official Publications of the European Communities
2009 – 44 pp. – 29.7 x 21.1 cm
EUR – Scientific and Technical Research series – ISSN 1018-5593
ISBN 978-92-79-12346-7
DOI 10.2790/11199

Abstract

The mechanisms controlling the migration of uranium in crystalline rocks such as granites or granodiorites are insufficiently well understood to arrive at a quantitatively defensible safety case for deep disposal of radioactive waste. To help further our knowledge of the relevant processes, a controlled column experiment was undertaken using a disc of metallic (depleted) uranium as a source and granodiorite samples from a former candidate disposal site for spent uranium fuel, Sievi in Finland, as the host medium. The experiment ran for approximately 500 days. This report summarises efforts made to simulate the uranium migration observed during the experiment. The model was developed from blind predictions to an inverse model that attempted to reproduce the measured effluent data. In the absence of independently derived kinetic data for uranium precipitation and dissolution it is difficult to arrive at a truly unique solution. Nevertheless, the exercise has been instructive in highlighting the principal areas of uncertainty and the pit falls that await those seeking to represent far more complex hydrogeochemical systems than that investigated here.

How to obtain EU publications

Our priced publications are available from EU Bookshop (http://bookshop.europa.eu), where you can place an order with the sales agent of your choice.

The Publications Office has a worldwide network of sales agents. You can obtain their contact details by sending a fax to (352) 29 29-42758.

The mission of the JRC is to provide customer-driven scientific and technical support for the conception, development, implementation and monitoring of EU policies. As a service of the European Commission, the JRC functions as a reference centre of science and technology for the Union. Close to the policy-making process, it serves the common interest of the Member States, while being independent of special interests, whether private or national.

JRC
EUROPEAN COMMISSION

LD-NA-23816-EN-C

ISBN 978-92-79-12346-7

Publications Office
Publications.europa.eu